



National Library
of Canada

Bibliothèque nationale
du Canada

Canadian Theses Service

Services des thèses canadiennes

Ottawa, Canada
K1A 0N4

CANADIAN THESES

THÈSES CANADIENNES

NOTICE

The quality of this microfiche is heavily dependent upon the quality of the original thesis submitted for microfilming. Every effort has been made to ensure the highest quality of reproduction possible.

If pages are missing, contact the university which granted the degree.

Some pages may have indistinct print especially if the original pages were typed with a poor typewriter ribbon or if the university sent us an inferior photocopy.

Previously copyrighted materials (journal articles, published tests, etc.) are not filmed.

Reproduction in full or in part of this film is governed by the Canadian Copyright Act, R.S.C. 1970, c. C-30. Please read the authorization forms which accompany this thesis.

**THIS DISSERTATION
HAS BEEN MICROFILMED
EXACTLY AS RECEIVED**

AVIS

La qualité de cette microfiche dépend grandement de la qualité de la thèse soumise au microfilmage. Nous avons tout fait pour assurer une qualité supérieure de reproduction.

S'il manque des pages, veuillez communiquer avec l'université qui a conféré le grade.

La qualité d'impression de certaines pages peut laisser à désirer, surtout si les pages originales ont été dactylographiées à l'aide d'un ruban usé ou si l'université nous a fait parvenir une photocopie de qualité inférieure.

Les documents qui font déjà l'objet d'un droit d'auteur (articles de revue, examens publiés, etc.) ne sont pas microfilmés.

La reproduction, même partielle, de ce microfilm est soumise à la Loi canadienne sur le droit d'auteur, SRC 1970, c. C-30. Veuillez prendre connaissance des formules d'autorisation qui accompagnent cette thèse.

**LA THÈSE A ÉTÉ
MICROFILMÉE TELLE QUE
NOUS L'AVONS REÇUE**

279

0-315-27020-9



National Library of Canada

Bibliothèque nationale du Canada

Canadian Theses Division / Division des thèses canadiennes

Ottawa, Canada K1A 0N4

PERMISSION TO MICROFILM - AUTORISATION DE MICROFILMER

Please print or type - Ecrire en lettres moulees ou dactylographier

Full Name of Author - Nom complet de l'auteur

NADIR YEGANI

Date of Birth - Date de naissance

05-11-1952

Permanent Address - Residence fixe

B 12120 103 AVE Edmonton, Alberta T5N 0P9

Country of Birth - Lieu de naissance

Istanbul - Turkey

Title of Thesis - Titre de la these

Experimental Analysis of The Laminar Flow Characteristics of Conical Bearings

University - Universite

University of Alberta

Degree for which thesis was presented - Grade pour lequel cette these fut presentee

MSc

Year this degree conferred - Annee d obtention de ce grade

1983

Name of Supervisor - Nom du directeur de these

Dr. J. S. Kennedy

Permission is hereby granted to the NATIONAL LIBRARY OF CANADA to microfilm this thesis and to lend or sell copies of the film

L'autorisation est, par la presente, accordee a la BIBLIOTHEQUE NATIONALE DU CANADA de microfilmer cette these et de prêter ou de vendre des exemplaires du film

The author reserves other publication rights, and neither the thesis nor extensive extracts from it may be printed or otherwise reproduced without the author's written permission

L'auteur se reserve les autres droits de publication, ni la these ni de longs extraits de celle-ci ne doivent être imprimés ou autrement reproduits sans l'autorisation écrite de l'auteur

Date

October 14/83

Signature

[Handwritten signature]

THE UNIVERSITY OF ALBERTA

Experimental Analysis Of The Laminar Flow Characteristics Of
Conical Bearings

by



Nadir Yegani

A THESIS

SUBMITTED TO THE FACULTY OF GRADUATE STUDIES AND RESEARCH
IN PARTIAL FULFILMENT OF THE REQUIREMENTS FOR THE DEGREE
OF Master of Science

Department Of Mechanical Engineering

EDMONTON, ALBERTA

Fall 1983

THE UNIVERSITY OF ALBERTA

RELEASE FORM

NAME OF AUTHOR Nadir Yegani
TITLE OF THESIS Experimental Analysis Of The Laminar
 Flow Characteristics Of Conical Bearings
DEGREE FOR WHICH THESIS WAS PRESENTED Master of Science
YEAR THIS DEGREE GRANTED Fall 1983

Permission is hereby granted to THE UNIVERSITY OF ALBERTA LIBRARY to reproduce single copies of this thesis and to lend or sell such copies for private, scholarly or scientific research purposes only.

The author reserves other publication rights, and neither the thesis nor extensive extracts from it may be printed or otherwise reproduced without the author's written permission.

(SIGNED).....

PERMANENT ADDRESS:

..#8..12120..103 AVE.....
..EDMONTON..ALBERTA...
..T5N..0P9.....

DATED ...October..14th...1983

THE UNIVERSITY OF ALBERTA
FACULTY OF GRADUATE STUDIES AND RESEARCH

The undersigned certify that they have read, and recommend to the Faculty of Graduate Studies and Research, for acceptance, a thesis entitled Experimental Analysis Of The Laminar Flow Characteristics Of Conical Bearings submitted by Nadir Yegani in partial fulfilment of the requirements for the degree of Master of Science.

.....*Kennedy*.....

Supervisor

.....*R. D. ...*.....

.....*...*.....

Date...*October 11, 1983*.....

TO MY WIFE

Abstract

This thesis describes an experimental investigation of the pressure distribution, load capacity and torque of the conical bearing with narrow gaps being constant, divergent and convergent.

The experiments were conducted for rotational and non-rotational states of the bearing slider, in the laminar flow regime with Reynolds numbers being less than 100.

The measurements are compared with a recent theoretical analysis which correlates the data within the experimental scatter. The experimental results presented show the dependence of the pressure distribution, load capacity and the torque on the bearing gap geometry. The load capacity and the torque for the convergent gaps are less than for divergent provided that the flow rate, rotation velocity and the film thickness at the outlet of the bearing gap are the same for both cases.

Acknowledgment

The author expresses his thanks to his supervisors Dr. Cz. M. Rodkiewicz and Dr. J. S. Kennedy for their guidance and advices during the preparation of the thesis, also thanks are due to Dr. W. Kalita for his assistance throughout this study.

Table of Contents

Chapter	Page
I. General Introduction	1
Introductory Remarks	1
Objectives Of The Thesis	2
II. A Survey Of The Literature	4
III. Theoretical Analysis	9
IV. Description Of Equipment	18
Experimental Procedure	22
V. Results and Discussion	25
VI. Observations	38
Suggestions For Further Work	41
VII. Tables	42
Bibliography	63
Appendix 1.	65
Experimental Error Estimation,	65
Appendix 2.	66
Calculation of Dimensionless Viscous Drag	66

List of Tables

Table	Page
VII.1 Dimensionless Pressure Distribution For Constant Gap Bearing.....	42
VII.2 Dimensionless Pressure Distribution For Constant Gap Bearing.....	43
VII.3 Dimensionless Pressure Distribution For Constant Gap Bearing.....	44
VII.4 Dimensionless Pressure Distribution For Constant Gap Bearing.....	45
VII.5 Dimensionless Pressure Distribution For Constant Gap Bearing.....	46
VII.6 Dimensionless Pressure Distribution For Constant Gap Bearing.....	47
VII.7 Dimensionless Pressure Distribution For Constant Gap Bearing.....	48
VII.8 Dimensionless Pressure Distribution For Constant Gap Bearing.....	49
VII.9 Dimensionless Pressure Distribution For Constant Gap Bearing.....	50
VII.10 Dimensionless Pressure Distribution For Convergent Gap Bearing.....	51
VII.11 Dimensionless Pressure Distribution For Convergent Gap Bearing.....	52
VII.12 Dimensionless Pressure Distribution For Convergent Gap Bearing.....	53
VII.13 Dimensionless Pressure Distribution For Convergent Gap Bearing.....	54
VII.14 Dimensionless Pressure Distribution For Convergent Gap Bearing.....	55
VII.15 Dimensionless Pressure Distribution For Convergent Gap Bearing.....	56
VII.16 Dimensionless Pressure Distribution For Divergent Gap Bearing.....	57

Table	Page
VII.17 Dimensionless Pressure Distribution For Divergent Gap Bearing.....	58
VII.18 Dimensionless Pressure Distribution For Divergent Gap Bearing.....	59
VII.19 Dimensionless Pressure Distribution For Divergent Gap Bearing.....	60
VII.20 Dimensionless Pressure Distribution For Divergent Gap Bearing.....	61
VII.21 Dimensionless Torque.....	62

List of Figures

Figure		Page
I.1	Journal-Thrust Bearing Arrangement.....	2
II.1	Coordinate System Of The Rotating Cone.....	6
II.2	Conical Bearing With Recess Depth.....	6
III.1	Conical Bearing Pad And Slider.....	9
III.2	Flow Separation.....	16
IV.1	Experimental Stand.....	18
IV.2	Conical Bearing Pad.....	19
IV.3	Runner Types.....	19
IV.4	Schematic Of Apparatus.....	22
IV.5	The Viscosity vs Temperature Curve.....	23
V.1	Dimensionless Pressure Distribution For Divergent Gap Bearing.....	26
V.2	Dimensionless Pressure Distribution For Constant Gap Bearing.....	27
V.3	Dimensionless Pressure Distribution For Convergent Gap Bearing.....	27
V.4	Dimensionless Pressure Distribution For Divergent, Constant and Convergent Gap Bearings.....	28
V.5	Rotational Effects On Dimensionless Pressure Distribution Of Constant Gap Bearing.....	30
V.6	Rotational Effects On Dimensionless Pressure Distribution Of Convergent Gap Bearing.....	31
V.7	Rotational Effects On Dimensionless Pressure Distribution Of Divergent Gap Bearing.....	32
V.8	Dimensionless Load Capacity.....	34
V.9	Dimensionless Load Capacity For Constant Gap Bearing.....	36
V.10	Dimensionless Load Capacity For Convergent Gap Bearing.....	36

Figure		Page
V.11	Dimensionless Load Capacity For Divergent Gap Bearing.....	37
V.12	The Torque Of The Conical Bearing.....	37

Nomenclature

a	Constant as indicated in equation (33)
b	Constant as indicated in equation (33)
c	Constant as indicated in equation (33)
F	Constant as indicated in equation (23)
h	Film thickness as indicated in Fig. III.1
h_0	Film thickness as indicated in Fig. III.1
\bar{h}	Dimensionless film thickness
\bar{k}	As defined by (8)
L	Load capacity
\bar{L}	Dimensionless load capacity
M	Torque
\bar{M}	Dimensionless torque
P	Pressure
P_0	Atmospheric pressure
P	Inlet pressure
\bar{P}	Dimensionless pressure
Q	Flow rate
R	As defined by (8)
Re	Reynolds number
Re_ω	Rotational Reynolds number
u	Velocity in x direction
\bar{u}	Dimensionless velocity in x direction
v	Velocity in y direction
\bar{v}	Dimensionless velocity in y direction
w	velocity in θ direction
\bar{w}	Dimensionless velocity in θ direction

x	Coordinate as indicated in Fig. III.1
\bar{x}	Dimensionless coordinate
\bar{x}_0	Coordinate as indicated in Fig. III.1
\bar{x}_1	Coordinate as indicated in Fig. III.1
\bar{y}	Coordinate as indicated in Fig. III.1
α	Cone angle as indicated in Fig. III.1
ϕ	Coordinate as indicated in Fig. III.1
ρ	Density
ν	Kinematic viscosity
ϵ	As defined by (3)
ψ	Cone angle as indicated in Fig. III.1
Ω	Rotational velocity

1. General Introduction

Introductory Remarks

Externally pressurized conical bearings¹ can in principle support a combination of radial and axial loads, and have superior load carrying advantages compared with other types of bearings. Over the past years they have been used for various purposes in the industry {1-3} such as:

- In centrifuges with high rotational velocity (centrifugal pumps, turbines).
- In vertical turbogenerators (in power stations).
- In vertical boring machines.
- In precision apparatus (eg. dynamometer) where the requirements are low friction and high accuracy.
- In telescopes to carry high load and permit easy rotation.

The reasons for the above listed industrial applications of conical bearings are that they are capable of carrying high loads and rotating relatively freely. Also by reducing axial and radial vibrations they provide high accuracy for sensitive precision apparatus.

Another application of conical bearings can be seen in "Journal-Thrust" bearing arrangement {3}. In this application they serve the same purpose (Fig.I.1).

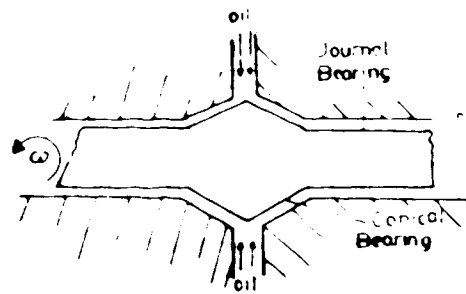


Figure 1.1 Journal+Thrust Bearing Arrangement

Objectives Of The Thesis

This thesis presents an experimental analysis of the performance of externally pressurized conical bearings with constant and non-constant film thicknesses.

Recently a theoretical analysis was conducted into the effect of non-constant film thickness on conical bearing characteristics [14]. The purpose of the experimental study described in this thesis was to obtain experimental data for comparison with the theoretical results of the above mentioned study. The objectives were to:

- Determine the flow characteristics and the performance (the load capacity and torque) of hydrostatically lubricated conical bearings for steady and rotational states with the bearing gaps, that is the space between the slider and the pad, being either constant, divergent or convergent.
- Investigate the flow separation (if any) on the bearing surfaces and its effects on the flow characteristics and the bearing performance.

- Discover any occurrence of turbulence in the flow within the range of Reynolds numbers from 25 to 75.
- Supply experimental data which can be useful for further studies on conical bearings.

II. A Survey Of The Literature

Numerous studies have been carried out on "Conical Bearings" over the past 50 years. The following survey of these studies is to provide the background necessary to understand the developments related with the analysis presented in this thesis.

C. M. Rodkiewicz and A. Mioduchowski [10] investigated the influence of the lubricant temperature in the conical bearing on the drag and on the load capacity of the bearing. By assuming that the value of viscosity was constant at a prescribed value and using an order of magnitude analysis, a reduced system of differential equations was formulated. This system of equations was solved with temperatures of slider and pad as parameters. They found that the temperature distribution along the lubricant film becomes significantly non-linear due to the effects of viscous dissipation. The influence of various temperatures of pad and slider on the temperature of the lubricant varies greatly depending upon the intensity of cooling. The decrease in the value of the viscosity reduces the values of the drag and the load capacity.

The flow created by a cone rotating in the air was investigated in the laminar flow regime by F. Kreith D. Ellis and J. Giesing [5]. Their experimental investigation was divided into two parts:

1. The analysis of the velocity distribution in the boundary layer.

2. The determination of the critical Reynolds number which exists at the transition from laminar to turbulent flow, and the influence of the cone vertex angle on the critical Reynolds number.

It was found that the velocity components predicted from boundary layer theory are in good agreement with the measured flow pattern for cones having vertex angles between 53.5 and 180 degrees. The transition from laminar to turbulent flow on a rotating cone is a function of the cone vertex angle and the rotational velocity.

Ching-Sheng Wu {4} studied analytically the motion induced in an incompressible viscous fluid by a spinning cone. In his analysis he showed that by appropriate transformations the equations describing the laminar boundary layer induced by a rotating cone can be reduced to the equations for laminar flow over a rotating disk; for which exact solutions are available in the literature. Another point of interest concerns the pressure distribution across the boundary layer. He found that the pressure at the solid wall decreases with increasing distance from the vertex. Therefore for a given value of the pressure outside the boundary layer there is a given value of x (Fig. II.1) beyond which the pressure at the surface becomes negative. This critical point may be considered to be the separation point of the boundary layer.

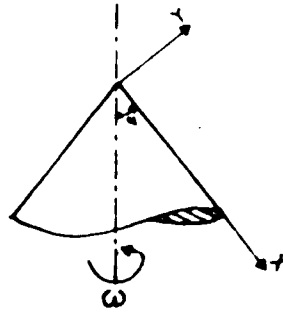


Figure II.1 Coordinate System Of The Rotating Cone

Essam Salem and Farid Khalil [12] presented both theoretical and experimental investigations of thermal effects on the performance (load capacity vs torque) of externally pressurized conical bearings. Experimental work was carried out to study the pressure distribution along the flow between the conical bearing elements and to verify the theoretical findings.

The analysis and the experimental results revealed that in the absence of rotation the isothermal and adiabatic solutions yield similar results for the bearing performance characteristics. However the deviation between the two solutions increases with decreasing film thickness, cone angle, recess depth (Fig.II.2), recess radius and with increasing rotational speed.

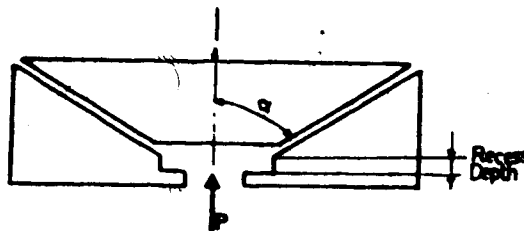


Figure II.2 Conical Bearing With Recess Depth

The increase in oil temperature that occurs increases the flow rate and has a detrimental effect on the load-carrying capacity.

Increasing the speed of rotation increases or decreases the load carrying capacity depending on the recess depth. Close agreement between the experimental results and the theory which includes inertia terms in the isothermal case is obtained for small rotational speeds.

C. M. Rodkiewicz, W. Jedruch and J. Skiepmo [11] analysed the dependence of viscosity on the temperature in an oil lubricated conical bearing. They found an increase in the load capacity when the temperature of the rotating part is continuously decreased from an arbitrary value (which is higher than the temperature of the stationary part) to some arbitrary value which is lower than the temperature of that part.

W. Kalita, J. S. Kennedy and C. M. Rodkiewicz [14] investigated the flow characteristics of a hydrostatically lubricated conical bearing with both constant and variable gaps between the stationary conical pad and the rotating slider. They determined the effect of the variable gap width on the flow characteristics and the performance of the bearing. The flow in the narrow gaps, that may be convergent or divergent, has been approximately determined on the basis of the lubrication theory.

It was found that for convergent gaps the pressure distribution along the gap differs significantly from the

results known for the case of constant film thickness. The load capacity and the torque for convergent gaps are lower than for divergent gaps, for given values of the rotational speed and film thickness.

III. Theoretical Analysis

In order to have an adequate understanding of the problem, a recent theoretical study{14} conducted on the subject (experimentally analysed in this study) is described below.

The analysis was carried out for viscous flow in the narrow gap of a conical bearing (Fig. III.1) with the distance h between the rotating slider and the stationary conical pad, being constant and non-constant.

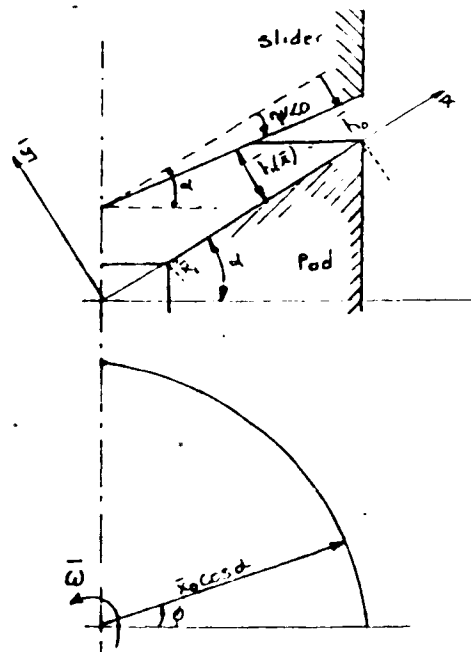


Figure III.1 Conical Bearing Pad and Slider

With the assumptions of:

- axial symmetry (i.e. all parameters are independent of the co-ordinate θ),
- isothermal and steady flow,
- constant density

and following Rodkiewicz and Mioduchowski {10} the flow

equations in the co-ordinate system (x, y, θ) , introduced in Figure III.1, were presented as:

$$\frac{\partial u}{\partial x} + \frac{\partial v}{\partial y} + \frac{u \cos \alpha - v \sin \alpha}{x \cos \alpha - y \sin \alpha} = 0$$

$$u \frac{\partial u}{\partial x} + v \frac{\partial u}{\partial y} + \frac{w^2 \cos \alpha}{x \cos \alpha - y \sin \alpha} = -\frac{1}{\rho} \frac{\partial p}{\partial x} + \nu \left\{ \frac{d^2 u}{dx^2} + \frac{d^2 u}{dy^2} + \frac{\frac{\partial u}{\partial x} \cos \alpha - \frac{\partial u}{\partial y} \sin \alpha}{x \cos \alpha - y \sin \alpha} - \frac{u \cos \alpha - v \sin \alpha}{(x \cos \alpha - y \sin \alpha)^2} \cos \alpha \right\}$$

$$u \frac{\partial v}{\partial x} + v \frac{\partial v}{\partial y} + \frac{w^2 \sin \alpha}{x \cos \alpha - y \sin \alpha} = -\frac{1}{\rho} \frac{\partial p}{\partial y} + \nu \left\{ \frac{d^2 v}{dx^2} + \frac{d^2 v}{dy^2} + \frac{\frac{\partial v}{\partial x} \cos \alpha - \frac{\partial v}{\partial y} \sin \alpha}{x \cos \alpha - y \sin \alpha} + \frac{u \cos \alpha - v \sin \alpha}{(x \cos \alpha - y \sin \alpha)^2} \right\} \quad (1)$$

$$u \frac{\partial w}{\partial x} + v \frac{\partial w}{\partial y} + w \frac{u \cos \alpha - v \sin \alpha}{x \cos \alpha - y \sin \alpha} = \nu \left\{ \frac{\partial^2 w}{\partial x^2} + \frac{\partial^2 w}{\partial y^2} + \frac{\frac{\partial w}{\partial x} \cos \alpha - \frac{\partial w}{\partial y} \sin \alpha}{x \cos \alpha - y \sin \alpha} - \frac{w}{(x \cos \alpha - y \sin \alpha)^2} \right\}$$

where u, v, w are the components of velocity in x, y, θ directions respectively, p is the pressure and α is the angle defined in Figure III.1.

The appropriate boundary conditions were:

$$u=v=w=0 \text{ at } y=0,$$

$$u=v=0, w=\omega(x \cos \alpha - y \sin \alpha) \text{ at } y=h(x) \quad (2)$$

Only the bearings with narrow gaps were considered with the

assumption of: λ

$$h = h_0 / x_0 \ll 1 \tag{3}$$

where h_0 is the reference distance between the pad and the slider and was chosen as: $h = h_0$ at $x = x_0$.

The velocity component v , across the gap, was assumed to be much smaller than the velocity component u , along the gap ($u \gg v$).

The characteristic (reference) velocities U, V, W for x, y and θ directions were presented as:

$$U = \frac{Q}{2\pi x_0 \rho_0 \cos\alpha}$$

$$V = \epsilon U \tag{4}$$

$$W = \omega x_0 \cos\alpha$$

Where Q is the dimensional flow rate through the bearing and ω is the angular velocity. Further with the dimensionless velocities:

$$\bar{w} = w/W, \bar{u} = u/U, \bar{v} = v/V \tag{5}$$

and with the following quantities:

$$\bar{x} = \frac{x}{x_0}, \bar{y} = \frac{y}{y_0}, \bar{h} = \frac{h}{h_0}$$

$$\bar{p} = \frac{(p - p_0) h_0^2}{\rho v^2 Re} \tag{6}$$

where $Re = Ux_0/v$, the flow equations were obtained as follows:

$$\frac{\partial \bar{u}}{\partial \bar{x}} + \frac{\partial \bar{v}}{\partial \bar{y}} + \frac{\bar{u} \cos\alpha}{\bar{x} \cos\alpha} - \frac{\epsilon \bar{v} \sin\alpha}{\epsilon \bar{y} \sin\alpha} = 0$$

$$\frac{\partial^2 \bar{u}}{\partial \bar{y}^2} - \frac{\partial \bar{p}}{\partial \bar{x}} + R \frac{\bar{w}^2 \cos \alpha}{\bar{x} \cos \alpha - \bar{y} \sin \alpha} = Re \epsilon^2 \left(\bar{u} \frac{\partial \bar{u}}{\partial \bar{x}} + \bar{v} \frac{\partial \bar{u}}{\partial \bar{y}} \right) + \epsilon \frac{\frac{\partial \bar{u}}{\partial \bar{y}} \sin \alpha - \epsilon \frac{\partial \bar{u}}{\partial \bar{x}} \cos \alpha}{\bar{x} \cos \alpha - \bar{y} \sin \alpha} + \epsilon^2 \left[\frac{\bar{u} \cos \alpha - \bar{v} \sin \alpha}{(\bar{x} \cos \alpha - \bar{y} \sin \alpha)^2} \cos \alpha - \frac{\partial^2 \bar{u}}{\partial \bar{x}^2} \right]$$

$$\frac{\partial \bar{p}}{\partial \bar{y}} = \epsilon^2 \frac{\partial^2 \bar{v}}{\partial \bar{y}^2} - \epsilon Re \frac{\bar{w}^2 \sin \alpha}{\bar{x} \cos \alpha - \bar{y} \sin \alpha} - \epsilon^2 \left(\bar{u} \frac{\partial \bar{v}}{\partial \bar{x}} + \bar{v} \frac{\partial \bar{v}}{\partial \bar{y}} \right) - \epsilon^3 \frac{\frac{\partial \bar{v}}{\partial \bar{y}} \sin \alpha - \epsilon \frac{\partial \bar{v}}{\partial \bar{x}} \cos \alpha}{(\bar{x} \cos \alpha - \bar{y} \sin \alpha)^2} \sin \alpha + \epsilon^4 \frac{\partial^2 \bar{v}}{\partial \bar{x}^2} \quad (7)$$

$$\frac{\partial^2 \bar{w}}{\partial \bar{y}^2} = Re \epsilon^2 \left(\bar{u} \frac{\partial \bar{w}}{\partial \bar{x}} + \bar{v} \frac{\partial \bar{w}}{\partial \bar{y}} + \bar{w} \frac{\bar{u} \cos \alpha - \bar{v} \sin \alpha}{\bar{x} \cos \alpha - \bar{y} \sin \alpha} \right) - \epsilon \frac{\frac{\partial \bar{w}}{\partial \bar{y}} \sin \alpha - \epsilon \frac{\partial \bar{w}}{\partial \bar{x}} \cos \alpha}{\bar{x} \cos \alpha - \bar{y} \sin \alpha} + \epsilon^2 \left[\frac{\bar{w}}{(\bar{x} \cos \alpha - \bar{y} \sin \alpha)^2} - \frac{\partial^2 \bar{w}}{\partial \bar{x}^2} \right]$$

where

$$R = Re_w^2 / Re, \quad Re_w = \bar{w} h_0 / (\text{rotational } Re \text{ number}) \quad (8)$$

The boundary conditions become:

$$\bar{u} = \bar{v} = \bar{w} = 0 \text{ at } \bar{y} = 0$$

$$\bar{u} = \bar{v} = 0, \quad \bar{w} = \bar{x} \text{ at } \bar{y} = \bar{h}(\bar{x}) \quad (9)$$

$$\bar{w} \cos \alpha = \bar{x} \cos \alpha - \bar{y} \sin \alpha \text{ at } \bar{y} = \bar{h}(\bar{x})$$

where $\bar{h}(\bar{x})$ determines the film thickness (the gap size)

which was defined as:

$$\bar{h} = \frac{(1 + \bar{k} \bar{x})}{(1 + \bar{k})} \quad (10)$$

where

$$\bar{k} = \tan \psi / (\epsilon - \tan \psi) \quad (11)$$

Bearings fulfilling the condition $-1 \leq \bar{k} \leq 2$ were considered, and it was assumed that for $\psi > 0$, $\tan \psi < \epsilon$.

The sign of the angle (ψ) was chosen in the following way:

k is

<0 for convergent gap

=0 for constant gap

(12)

>0 for divergent gap

The equations (7) and the conditions (9) were simplified under the assumption (3). Only the terms of order ϵ were maintained. Additionally it was assumed that the angle α is not close to 90° and all terms on the left-hand sides of equations (7) were to be maintained.

Under these assumptions the simplified flow equations were presented in the following dimensionless form:

$$\frac{\partial \bar{u}}{\partial \bar{x}} + \frac{\partial \bar{v}}{\partial \bar{y}} + \frac{\bar{u}}{\bar{x}} = 0$$

$$\frac{\partial^2 \bar{u}}{\partial \bar{y}^2} - \frac{\partial \bar{p}}{\partial \bar{x}} + R \frac{\bar{w}^2}{\bar{x}} = 0$$

(13)

$$\frac{\partial \bar{p}}{\partial \bar{y}} = 0$$

$$\frac{\partial^2 \bar{w}}{\partial \bar{y}^2} = 0$$

From the third of equations (13) it follows that $\bar{p} = \bar{p}(\bar{x})$ and from the fourth equation applying the appropriate boundary conditions in (9):

$$\bar{w} = \bar{x}\bar{y}/\bar{h}(\bar{x})$$

(14)

\bar{u} was obtained from the second equation in (13) to be:

$$\bar{u} = \frac{1}{2} \bar{p}' \bar{y} (\bar{y} - \bar{h}) - \frac{1}{12} R \frac{\bar{x}\bar{y}}{\bar{h}^2} (\bar{y}^3 - \bar{h}^3)$$

(15)

From the continuity equation in (13), \bar{v} was determined to be

$$\bar{v} = \frac{1}{2} \frac{d(\bar{h}^3)}{d\bar{x}} \quad (16)$$

$$\bar{v} = \frac{3}{2} \bar{h}^2 \left(\bar{h}' - \bar{x} \bar{h}'' \right) \quad (17)$$

where each prime indicates differentiation with respect to \bar{x} .

Using the boundary condition $\bar{v}=0$, at $\bar{y}=\bar{h}$ the pressure distribution along the gap is:

$$(\bar{p}' \bar{x} \bar{h}^3)' = \frac{3}{10} R (\bar{h}^3 \bar{x}^2)' \quad (18)$$

which when solved with the following boundary conditions:

$$\left. \begin{array}{l} \bar{p}=0 \\ \int_0^1 \bar{u} d\bar{y}=1 \end{array} \right\} \quad \text{at } \bar{x}=1 \quad (18)$$

yields

$$\bar{p} = 12\bar{g}(\bar{x}, \bar{k}) - (3/20)R(1-\bar{x}^2) \quad (19)$$

where the function $\bar{g}(\bar{x}, \bar{k})$ was given by:

$$\bar{g}(\bar{x}, \bar{k}) = (1 + \bar{k})^3 \left\{ \ln \frac{1 + \bar{k}\bar{x}}{\bar{x}(1 + \bar{k})} + \frac{1}{2} \left[\left(\frac{2 + \bar{k}}{1 + \bar{k}} \right)^2 - \left(\frac{2 + \bar{k}\bar{x}}{1 + \bar{k}\bar{x}} \right)^2 \right] \right\} \quad (20)$$

The load capacity for the geometry presented in Fig.4 in dimensionless form was defined as:

$$\bar{L} = \bar{p}_1 \bar{x}_1^2 + 2 \int_0^1 \bar{p} \bar{x} d\bar{x} \quad (21)$$

where the first term accounts for the inlet pressure (\bar{p}_1) and the second for the lifting force created along the gap of the bearing. The contribution of the viscous stresses into the value of the lifting force was neglected in (21) due to the assumption that ϵ was a small quantity much less than 1.

Using the pressure given by (19) in equation (21) yields:

$$\bar{L} = 12\bar{F}(\bar{x}_1, k) (3 - 20)R(1 - \bar{x}_1^2) \quad (22)$$

where

$$\bar{F}(\bar{x}_1, k) = (1+k)(1-\bar{x}_1)(1+\bar{x}_1+2k\bar{x}_1)(1+k\bar{x}_1)^2 \quad (23)$$

The torque of the bearing in dimensionless form was defined as:

$$\bar{M} = \frac{1}{4} \frac{1+k}{k} \frac{1}{h^2} \frac{d\bar{w}}{d\bar{x}} \quad (24)$$

and for the bearings considered was equal to:

$$\bar{M} = \frac{1+k}{4k} \left[\frac{1+k\bar{x}_1}{1+k} + \frac{k^3}{3} (1 - \bar{x}_1^3) - \frac{k^2}{2} (1 - \bar{x}_1^2) + k(1 - \bar{x}_1) \right] \quad (25)$$

The solution for the \bar{u} component of velocity in (15) indicates the possibility of flow separation in the gap.

From equation (15) it was found that:

$$\frac{\partial \bar{u}}{\partial \bar{y}} = \begin{cases} \frac{6}{\bar{x}} \frac{1}{h^2} - \frac{R}{15} \bar{x} \bar{h}, & \text{at } \bar{y} = 0 \\ -\frac{6}{\bar{x}} \frac{1}{h^2} - \frac{R}{10} \bar{x} \bar{h}, & \text{at } \bar{y} = \bar{h} \end{cases} \quad (26)$$

From the condition determining the points of separation [7] at the surfaces of the bearing

$$\frac{\partial \bar{u}}{\partial \bar{y}} \Big|_{\substack{\bar{y} = 0 \\ \bar{y} = \bar{h}}} = 0 \quad (27)$$

and it follows that for the slider surface, $\bar{y} = \bar{h}$, the value $\frac{d\bar{u}}{d\bar{y}}$ is always negative.

Then the points of separation can be present only at the pad surface for \bar{x} determined by:

$$R\bar{x}^{-2} \left[\frac{1+k\bar{x}}{1+k} \right]^3 = 90 \quad (28)$$

It was also concluded that the separation of flow (Fig. III.2) would occur for any gap geometry and for all rotating bearing conditions when:

$$R > 90 \quad (29)$$

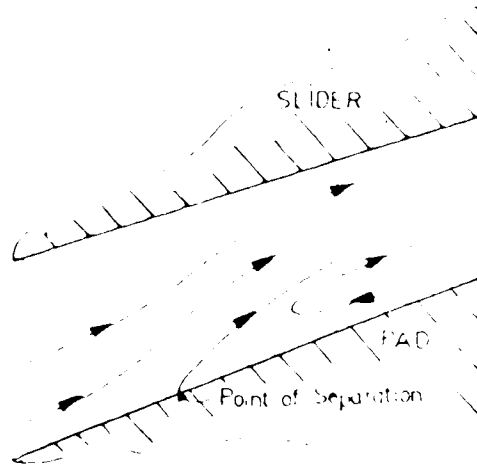


Figure III.2 Flow Separation

Under these conditions the pressure in some part of the gap, close to the outlet, becomes less than the pressure at the outlet due to centrifugal forces created by the rotating slider.

It can be noticed that with the increasing velocity of rotation the load capacity of the bearing decreases and may approach to the zero value for:

$$R = 80 \frac{(1 + k)(1 + x_1 + 2\bar{k}\bar{x}_1)}{(1 + \bar{x}_1^2)(1 + \bar{x}_1)(\bar{k} + \bar{k}\bar{x}_1)^2} \quad (30)$$

In particular for the constant gap bearing ($\bar{k}=0$) it follows from (30) that the zero load capacity was obtained for $R \approx 80$, if the value of \bar{x} was relatively small compared with 1. Then taking into account the condition (29) it may be concluded that the separation of laminar flow in the

constant gap bearings would not occur in practical situations, where the axial displacement of the bearing's slider is not restricted.

IV. Description Of Equipment

The conical thrust bearing was basically composed of a pad and runner (Fig. IV.1).

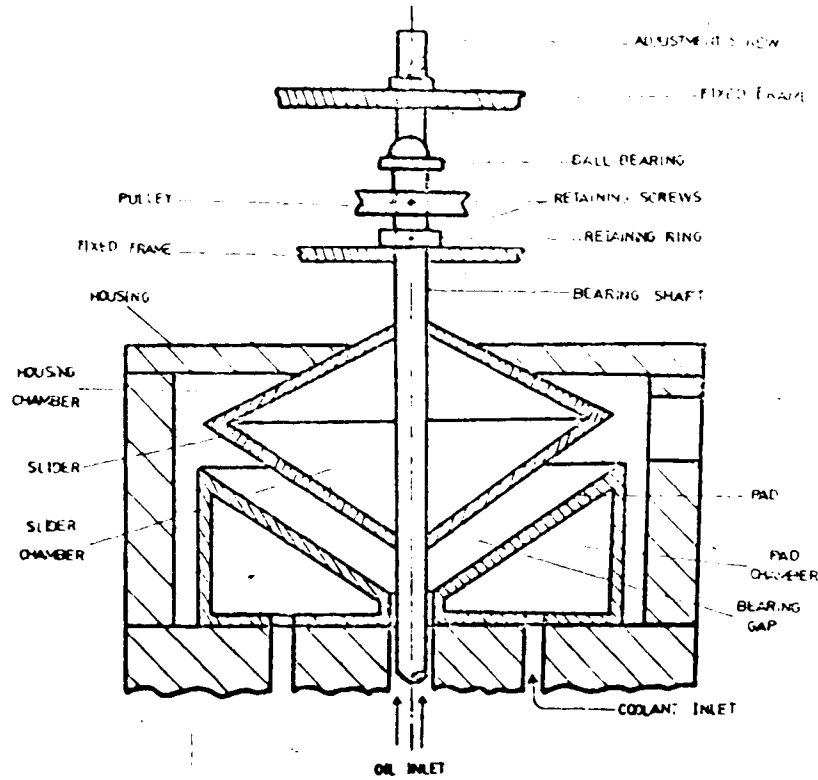


Figure IV.1 Experimental Stand

The V-shaped pad was equipped (Fig. IV.2) with six temperature probes, one turbulence probe and six pressure taps. The outlets of these taps were connected to the pressure transducers via plastic tubes. An oil supply hole was located at the center of the pad where a small plastic thrust bearing was mounted to hold the runner's shaft in

alignment.

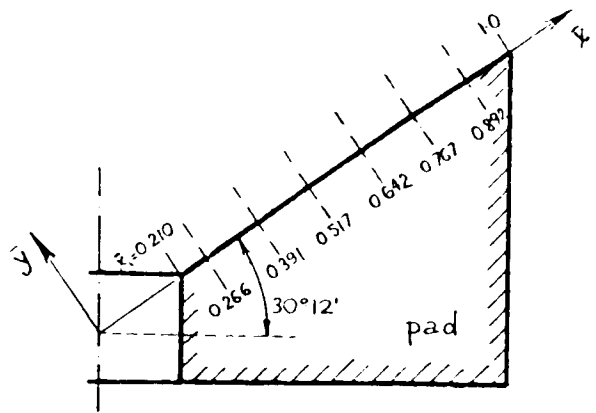


Figure IV.2 Conical Bearing Pad

The runner was also V-shaped to fit into the concave pad. A shaft extended through and was fastened to this runner. The runner was rotated by a D-C electrical motor using a pulley-belt drive. The pulley was attached to the top end of the runner's shaft. The axial movement of the runner was controlled by a ball bearing and a retaining ring fastened to the shaft respectively above and below the pulley.

A restraining bolt which rested upon the ball bearing was fastened firmly to a fixed plate. Three different types of runner were used during the experiments (Fig. IV.3).

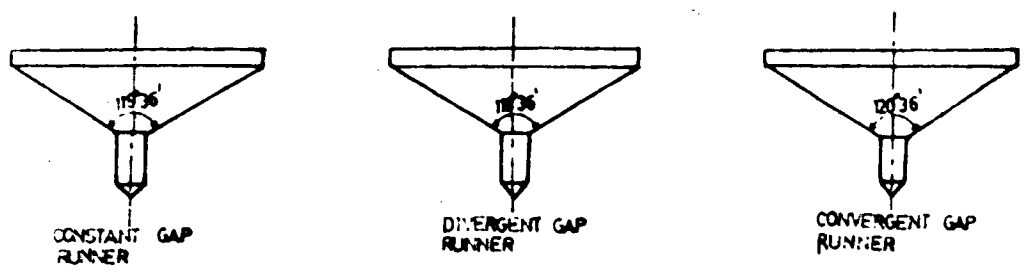


Figure IV.3 Runner Types

The pad and the runner were installed in a housing unit.

A dial gauge set on the top of the restraining bolt was used to measure the changes in the gap width, feeler gauges were utilised to obtain the desired gap thickness.

A control rheostat in the electric circuit was used to change the rotational speed. The exact rotational speed was measured with a photo-electric rotatiometer.

The power consumption of the electrical motor was measured with the use of a voltmeter and a current-meter installed in the electric circuit.

The oil used in the experiment was "SAE 30" motor lubrication oil and it was supplied to the bearing by a constant flow pump. It entered the bearing from the oil supply hole and returned to the pump via an outlet pipe on the side of the housing unit and a reservoir tank. The flow through the bearing was determined by the regulating and bypass valves. The flow rate was measured by timing a given amount of oil collected in a beaker.

A thermometer placed in the oil reservoir was utilised to monitor the average oil temperature.

The pressure taps were connected to a "Valydine pressure transducer" through a switchboard equipped with six needle valves; a particular pressure reading was obtained by switching on the corresponding valve. The transducer was connected to a voltmeter via a "sine wave carrier demodulator" which provided a d-c output signal to the voltmeter. The voltmeter output was converted to pressure.

The turbulence effect was observed using a "Hot wire anemometer" which is especially suited for measuring high frequency flow fluctuation. The hot-wire probe is primarily sensitive to the component of flow velocity that is normal to the wire. With the hot-wire mounted vertically with respect to the direction of mean flow, the fluctuating component of the hot-wire signal (available at the output terminal) corresponds, in the main, to the fluctuating component of the longitudinal flow velocity. The principle of measurement is based on the convective heat loss from an electrically heated wire caused by the flow of liquid surrounding the wire.

Experimental Procedure

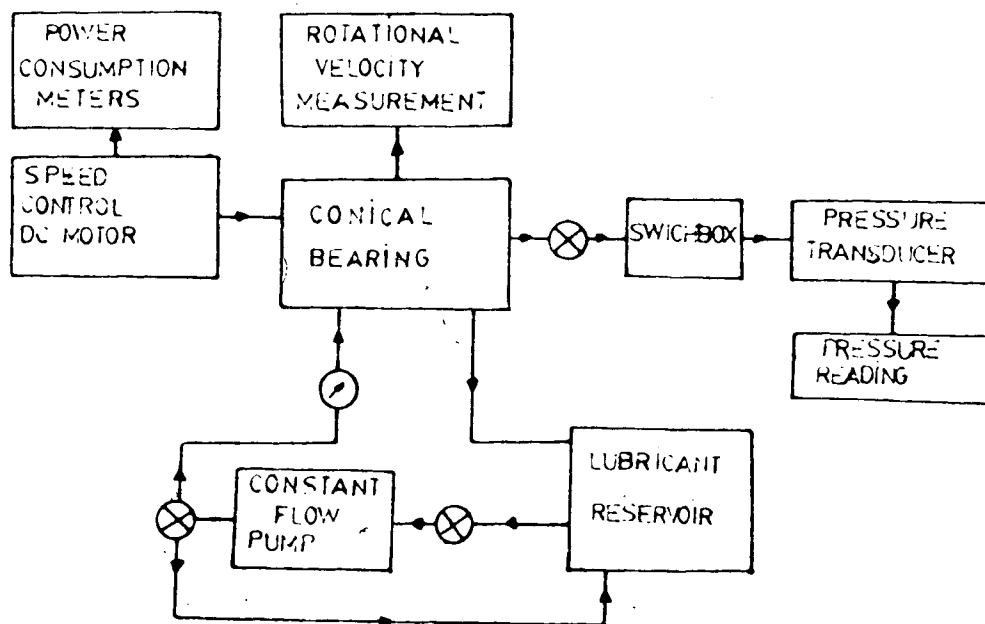


Figure IV.4 Schematic Of Apparatus

In order to reduce the number of parameters affecting the flow characteristics, the experiments were based on the Reynolds number, for a particular gap size. The three groups of Reynolds numbers selected for the experiments were $Re=25$, $Re=50$, $Re=75$.

The controlling quantities were: k defined through equation (11) determining the geometry of the bearing, and R defined through (8) determining the effect of the inertia force due to rotation with respect to the effects of flow derived from the pressure gradient along the gap.

The resulting quantities were: the dimensionless pressure

distribution along the gap and the torque of the bearing. The load capacity for the interval $\bar{x}_1 \leq \bar{x} \leq \bar{x}_0$ along the bearing gap was calculated from the pressure distribution.

To minimize the experimental error, the variations on the gap size were limited for a minimum of 0.65 mm and for a maximum of 1.27 mm. For gap sizes lower than 0.55 mm the experimental stand was subject to elastic deformations due to the force generated by high oil pressure in the bearing. For gap sizes higher than 1.32 mm the oil pressure obtained was so low that it could not be measured with available equipment. Although the range of the gap size was limited, it was sufficient to fulfill the aim of the thesis.

For convergent and divergent gaps the four different geometric factors used were: $\bar{k}=-0.4$, $\bar{k}=-0.5$ for convergent gap and $\bar{k}=1.5$ and $\bar{k}=2.00$ for divergent gap.

A viscosity versus temperature curve of the oil utilized was obtained in order to make the necessary adjustments on the flow rate varying with increasing oil temperature (Fig. IV.5)

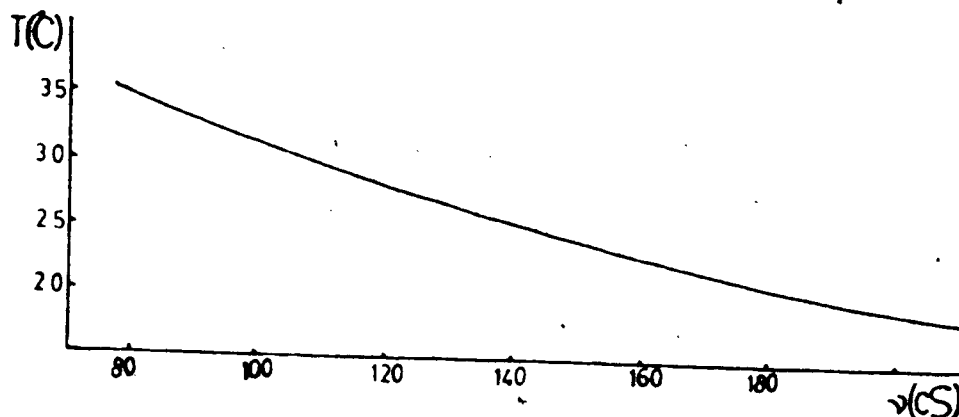


Figure IV.5 The Viscosity vs Temperature Curve

The flow rate was set to achieve a selected Reynolds number. During each run the oil temperature was continuously observed and for decreasing viscosity the necessary variations on the flow rate were made in order to maintain a constant Reynolds number.

The density of the oil used was measured for various temperatures and assumed constant (the change observed was in the range of 2%).

The pressure transducer was calibrated to provide 1 volt per 6.895 kpa (1 lb/sq in) and was found to be linear. The pressure measurements were taken for rotational states of the bearing varying between zero and 1000 rpm. The maximum rotational speed obtained was 1000 rpm (reached using increments of 250 rpm).

The drag measured during the experiments was the total drag (viscous drag + drag generated by the equipment). To obtain the drag caused only by the equipment a certain gap was set and the bearing was run without any oil flow through it. Later these results were subtracted from the total drag to obtain the viscous drag. (see appendix 2 for calculations)

The calculated experimental error was 17%. (see appendix 1)

V. Results and Discussion

The effect of non-constant film thickness along the gap of the bearing and the effect of rotation on the flow characteristics, load capacity and the torque, of the bearing were considered during the experiments.

Figures V.1, 2, 3 and 4 present the theoretical and experimental pressure distributions for bearings with divergent ($k > 0$), constant ($k = 0$) and convergent ($k < 0$) gaps, for non-rotational conditions. The theoretical solid curves present the function $\bar{g}(\bar{x}; \bar{k})$ defined through (20). It can be seen that for divergent and constant gap bearings (Figs. V.1 and 2) the agreement between the experimental results and the theory is very close. However, for convergent gap bearing (Fig. V.3) the experimental pressure values are higher than the theoretical values. The agreement between the theory and the experiment is qualitative rather than quantitative, that is, the theoretical and experimental profiles are similar but are not numerically the same. The discrepancy between the experimental results and the theory might be due to the fact that some viscous drag terms were neglected in the simplification of the flow equations (13). The pressure distributions obtained for the same value of \bar{k} but different values of Reynolds numbers are very close to each other. It may be concluded that in the range of laminar flow, for Re values from 25 to 75, the influence of Reynolds number on dimensionless pressure distribution is actually not important.

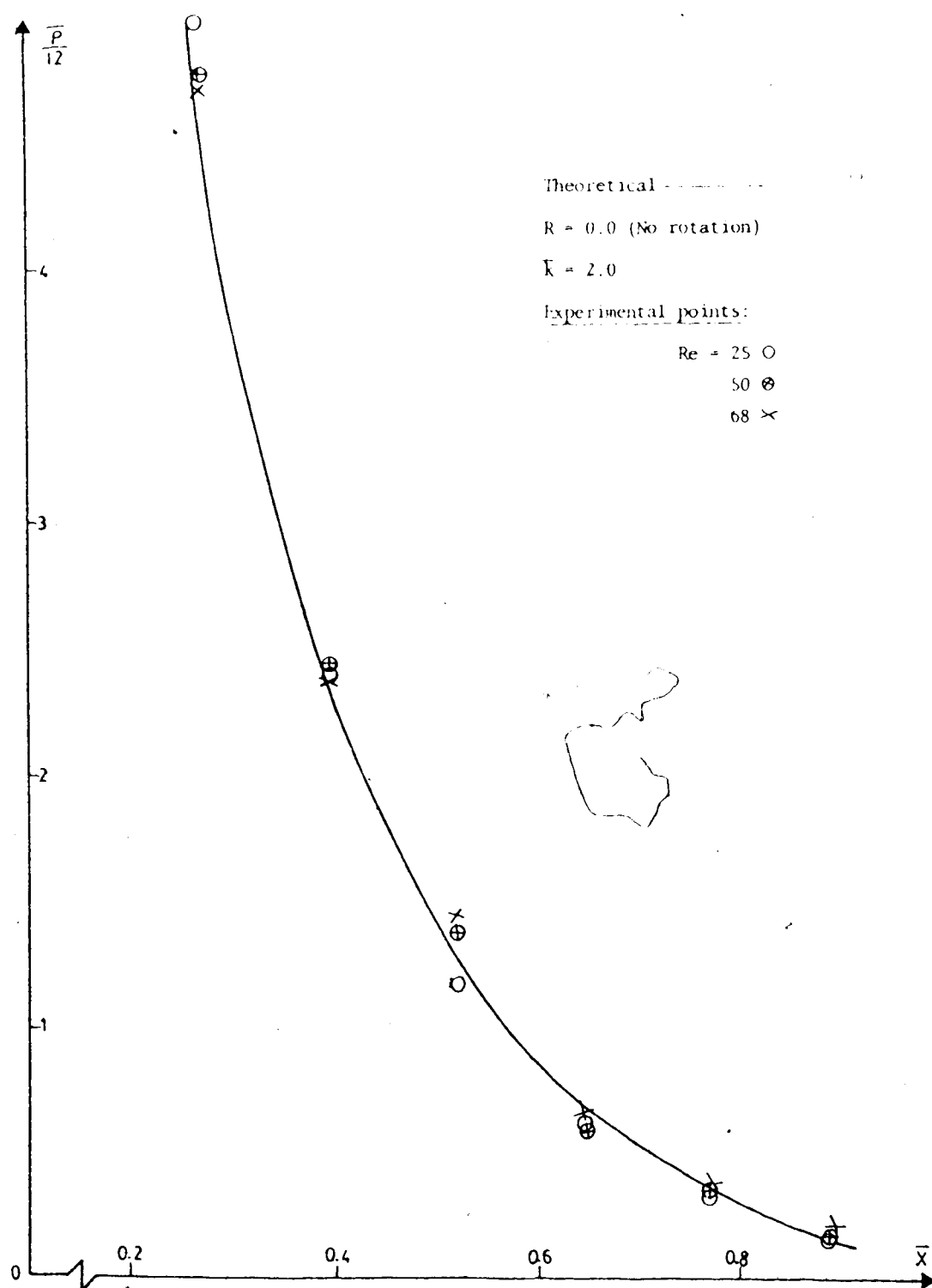


Figure V.1 Dimensionless Pressure Distribution For Divergent Gap Bearing

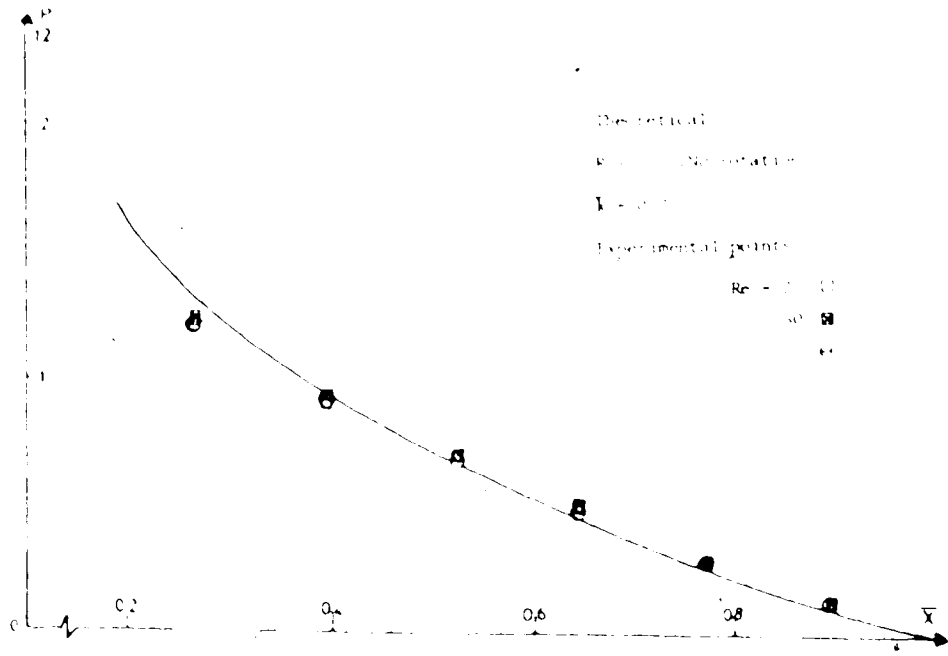


Figure V.2 Dimensionless Pressure Distribution For Constant Gap Bearing

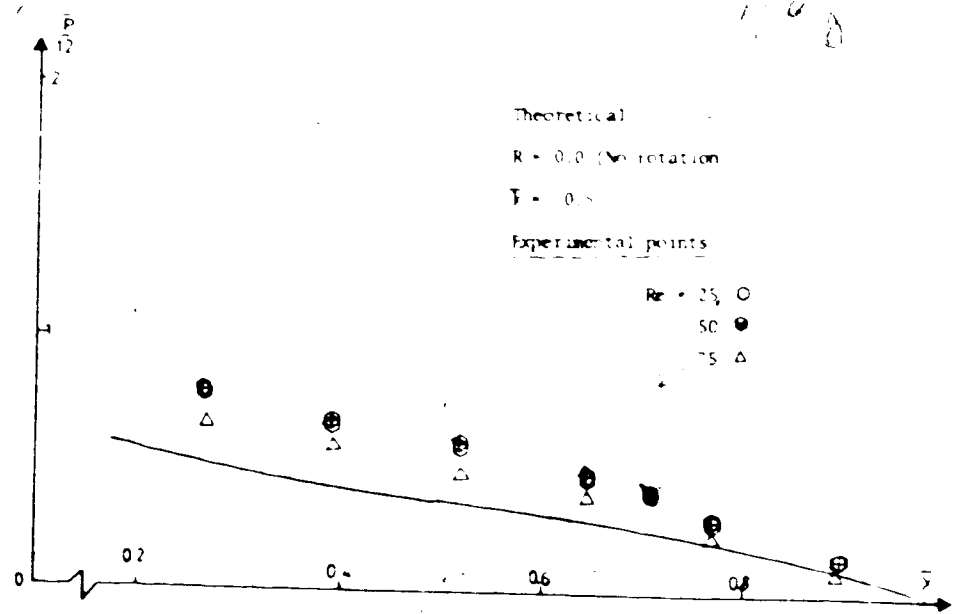


Figure V.3 Dimensionless Pressure Distribution For Convergent Gap Bearing

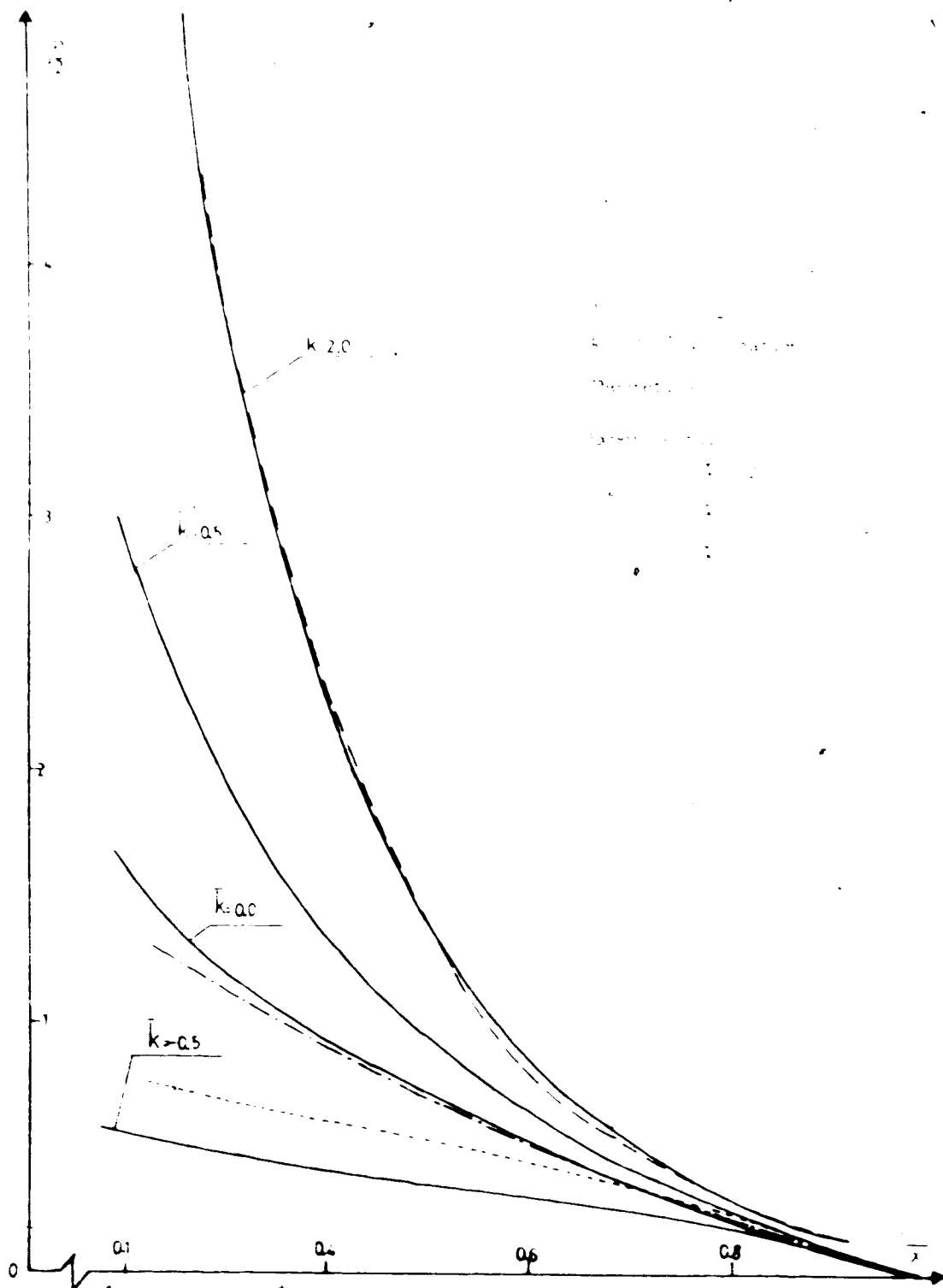


Figure V.4 Dimensionless Pressure Distribution For Divergent, Constant and Convergent Gap Bearings

The theoretical and experimental pressure distributions along the gap for constant ($k=0$), convergent ($k=0.4$) and divergent ($k=1.5$) film thicknesses and with variable values of the parameter R , representing the rotational effect, are given respectively in Figures V.5, 6 and 7. The theoretical curves shown by solid lines were obtained using the expression (19). As the parameter R increases a progressive increase can be seen in the difference between the theoretical and experimental pressure distributions.

For higher values of the parameter R the dimensionless pressure reaches negative values along the greater part of the bearing gap. In addition it was noted that the experimental pressure profiles have inflexion points in the negative pressure region. This may be observed in particular for $R=152.5$, in the case of constant gap (Fig. V.5), and for $R=185.3$, in the case of convergent gap (Fig. V.6). It may be concluded that the separation of the flow in the gap, predicted in the theoretical analysis, is responsible for this effect.

For the bearing with divergent gap (Fig. V.7) the dimensionless experimental pressure distribution is considerably lower than the theoretical distribution close to the bearing gap inlet. This discrepancy might be caused by the neglecting of some inertia terms in the theoretical analysis. The theoretical load capacity (22) was found for the bearing with simplified geometry shown in Figure III.1. The actual test bearing had more complex geometry at the

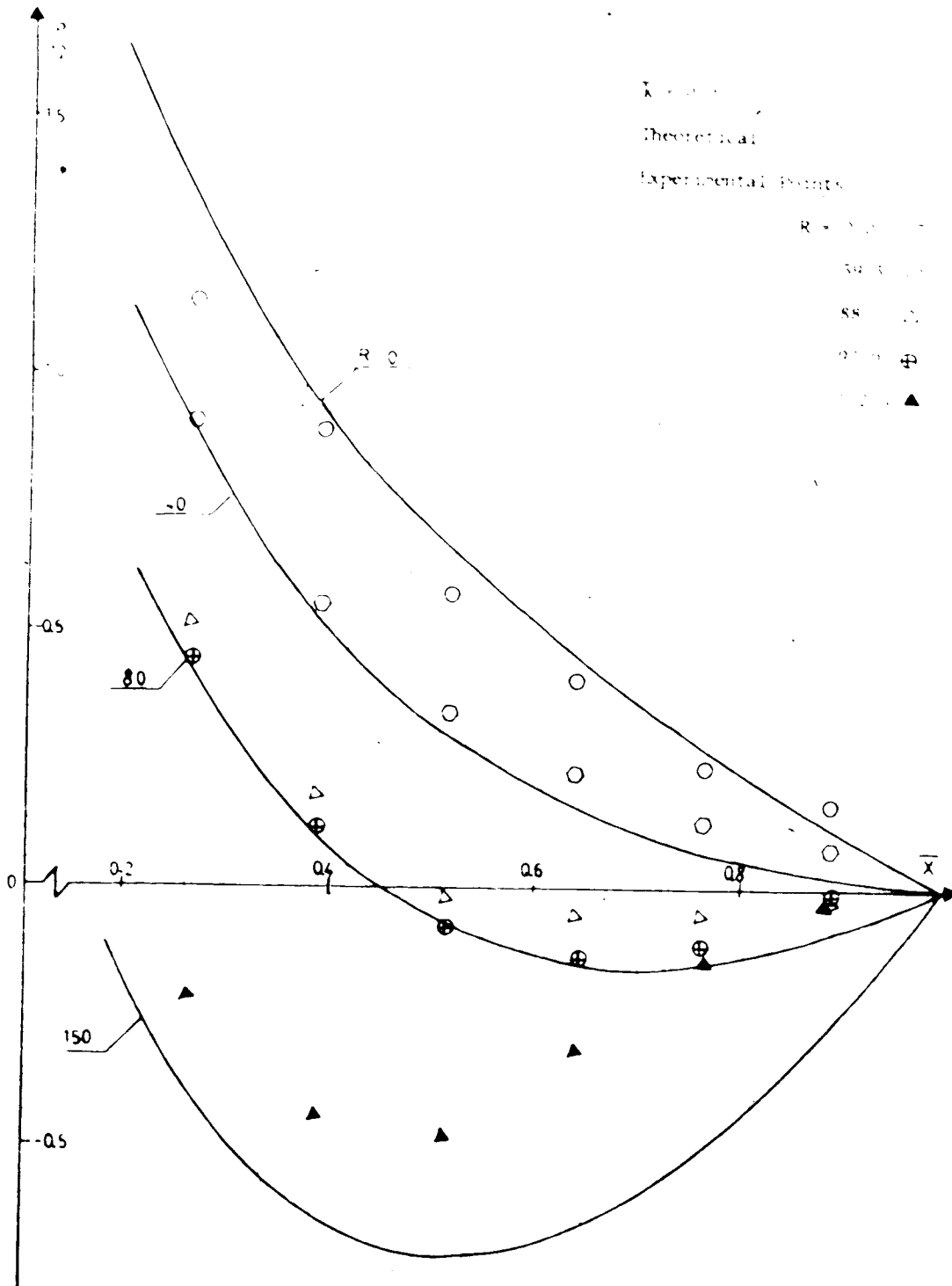


Figure V.5 Rotational Effects On Dimensionless Pressure Distribution Of Constant Gap Bearing

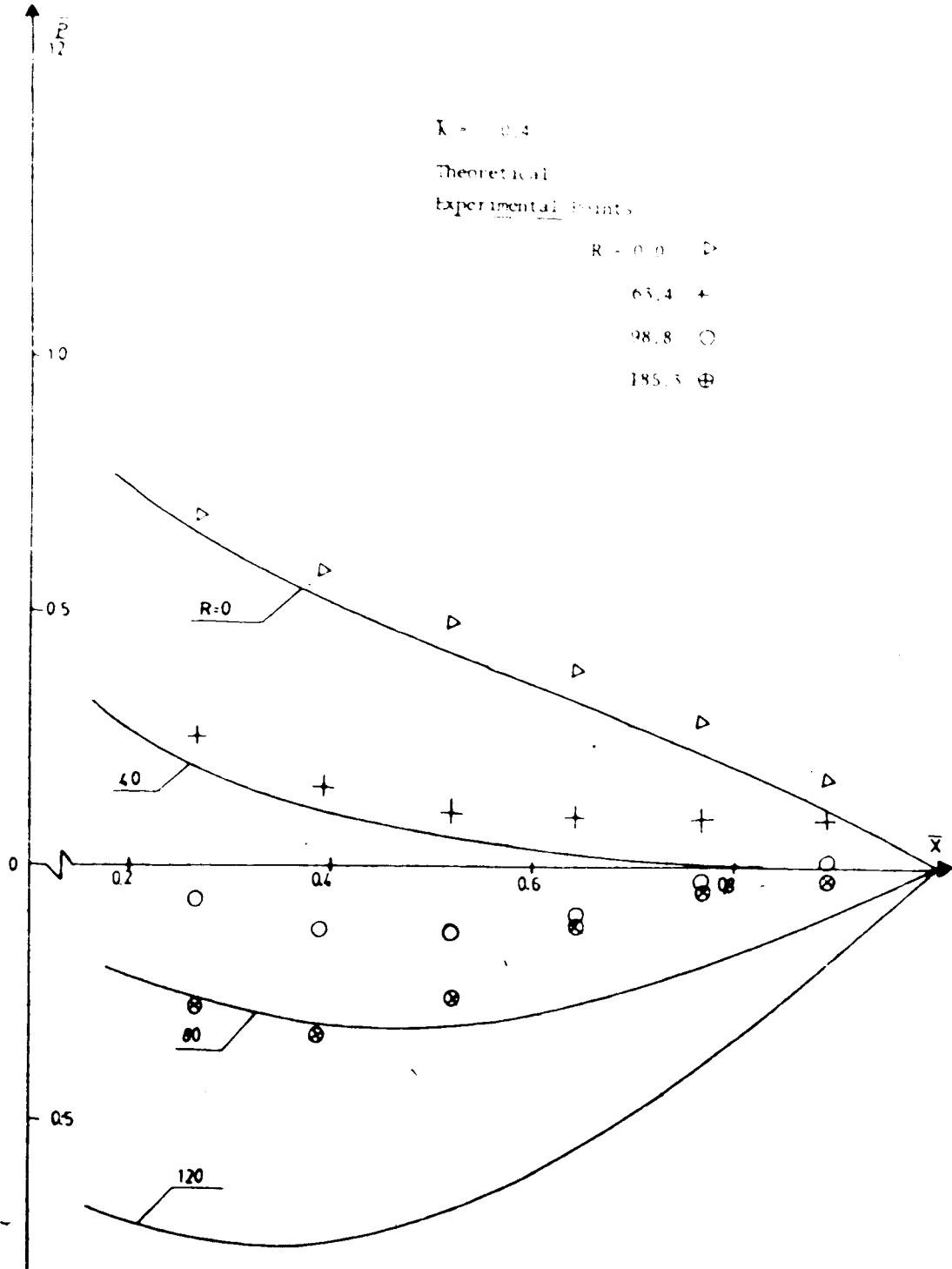


Figure V.6 Rotational Effects On Dimensionless Pressure Distribution Of Convergent Gap Bearing

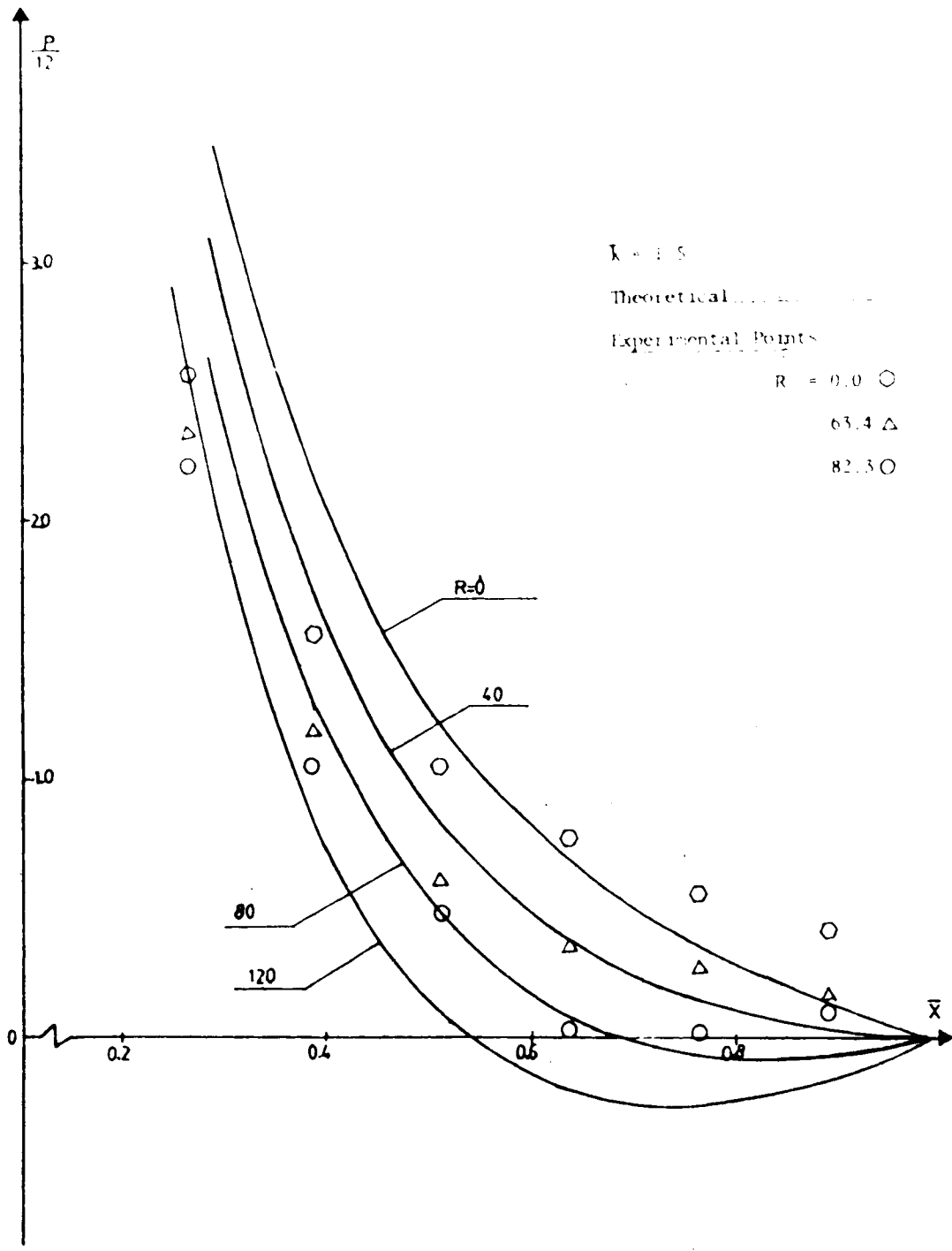


Figure V.7 Rotational Effects On Dimensionless Pressure Distribution Of Divergent Gap Bearing

inlet part of the gap. For this reason, only the load capacity created in the conical part of the bearing for the interval $\bar{x}_1 \leq \bar{x} \leq \bar{x}_6$ was considered instead of the theoretical expression (22), obtained in Section 3.

As a result the following theoretical load capacity {15} was obtained:

$$\bar{L}_{p \text{ th}} = \frac{1}{12} \int_{\bar{x}_1}^{\bar{x}_6} \bar{p} \bar{x} d\bar{x} = \int_{\bar{x}_1}^{\bar{x}_6} \left[\bar{g}(\bar{x}; k) - \frac{R}{80} (1 - \bar{x}^2) \right] \bar{x} d\bar{x} \quad (31)$$

where x_1 and x_6 were the dimensionless coordinates of the pressure measurement points at the stationary pad (Fig. IV.2).

By integrating (31) the following expression for the theoretical load capacity {15} was obtained:

$$\begin{aligned} \bar{L}_{p \text{ th}} = & (1 + k)^3 \left\{ \frac{\bar{x}_6^2}{2} \ln \frac{1 + k\bar{x}_6}{\bar{x}_6(1+k)} - \frac{\bar{x}_1^2}{2} \ln \frac{1 + k\bar{x}_1}{\bar{x}_1(1+k)} \right. \\ & + \frac{\bar{x}_6^2 - \bar{x}_1^2}{4} \left[1 + \left(\frac{2+k}{1+k} \right)^2 \right] - \frac{\bar{x}_6}{2k} (1 + k\bar{x}_6) + \frac{\bar{x}_1}{2k} (1 + k\bar{x}_1) \\ & \left. - \frac{1}{2k^2} \left(\frac{1}{1+k\bar{x}_6} - \frac{1}{1+k\bar{x}_1} \right) \right\} - \frac{R}{160} \left[\bar{x}_6^2 \left(1 - \frac{\bar{x}_6^2}{2} \right) - \bar{x}_1^2 \left(1 - \frac{\bar{x}_1^2}{2} \right) \right] \end{aligned} \quad (32)$$

For calculation of the experimental values of the load capacity for the interval $x_1 \leq x \leq x_6$ a parabolic mean-square regression of second order, for the experimental pressure distribution {15}, was assumed in the range (\bar{x}_1, \bar{x}_6) in the form of

$$\bar{p}/12 = a\bar{x}^2 + b\bar{x} + c \quad (33)$$

where the coefficients a , b and c were estimated by the

capacity was obtained [15] as follows:

$$\bar{L}_{pe} = \int_{\bar{x}_1}^{\bar{x}_6} (a\bar{x}^2 + b\bar{x} + c) \bar{x} d\bar{x} = \frac{a}{4} (\bar{x}_6^4 - \bar{x}_1^4) + \frac{b}{3} (\bar{x}_6^3 - \bar{x}_1^3) + \frac{c}{2} (\bar{x}_6^2 - \bar{x}_1^2) \quad (34)$$

The theoretical and the experimental load capacities for the interval $\bar{x}_1 \leq \bar{x} \leq \bar{x}_6$ are plotted against the parameter \bar{k} (for non-rotational conditions) is presented in Figure V.8. The experimental and theoretical values of the load capacity \bar{L} are very close to each other, for constant and divergent gap bearings. This follows from the pressure distributions in Fig.V.4. For the convergent gap bearing ($\bar{k} = -0.5$) the experimental load capacities are higher than the theoretical values by as much as 30%. In the range of the experimental Reynolds numbers from 25 to 75 no evident influence of the experimental Re number on dimensionless load capacity was observed.

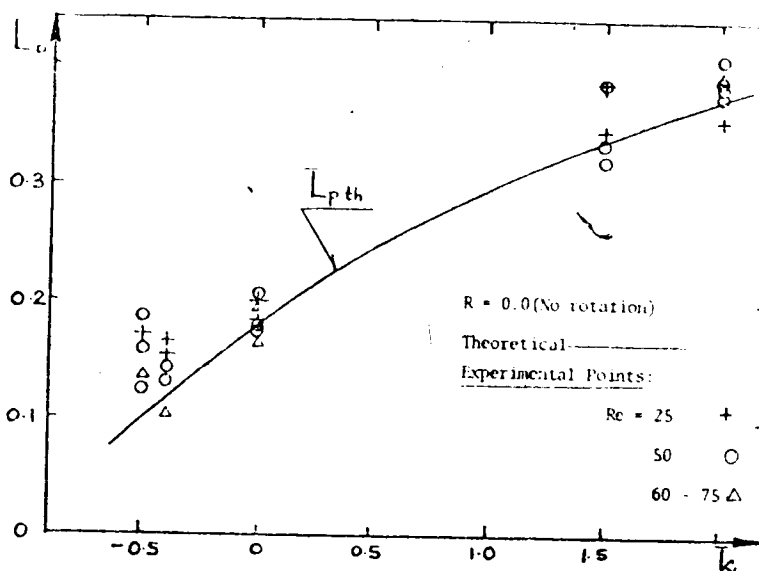


Figure V.8 Dimensionless Load Capacity

The effects of the rotational parameter R on the load capacity for constant, convergent and divergent gaps are presented in Figures V.9, 10 and 11 respectively. The theoretical load capacities (solid lines) were obtained from the expression (31). It can be noticed that with the increase of rotation at $R > 80$, the experimental load capacities are higher than predicted theoretical values. One possible reason for these discrepancies could be the flow separation in the bearing gap.

The results of the calculations of the torque, based on the measurements of the bearing's power consumption, are given in the Table VII.21 (see chapter VII). No evident relationship between the torque \bar{M} and the parameters Re or R was found during the analysis. The torque seems to be dependent only on the geometrical parameter \bar{k} as predicted by the theory. The variations of the torque (\bar{M}) for different values of the parameter k are given in Figure V.12, where the selected rotational velocities (Ω) are indicated. The theoretical solid line in that figure follows the expression (25) for $\bar{x}=0.210$.

For the constant gap geometry the experimental and theoretical values of torque are close to each other, while for the bearings with non-constant film thicknesses they differ by up to 20% from each other.

During the experiments no sign of turbulence in the flow was found.

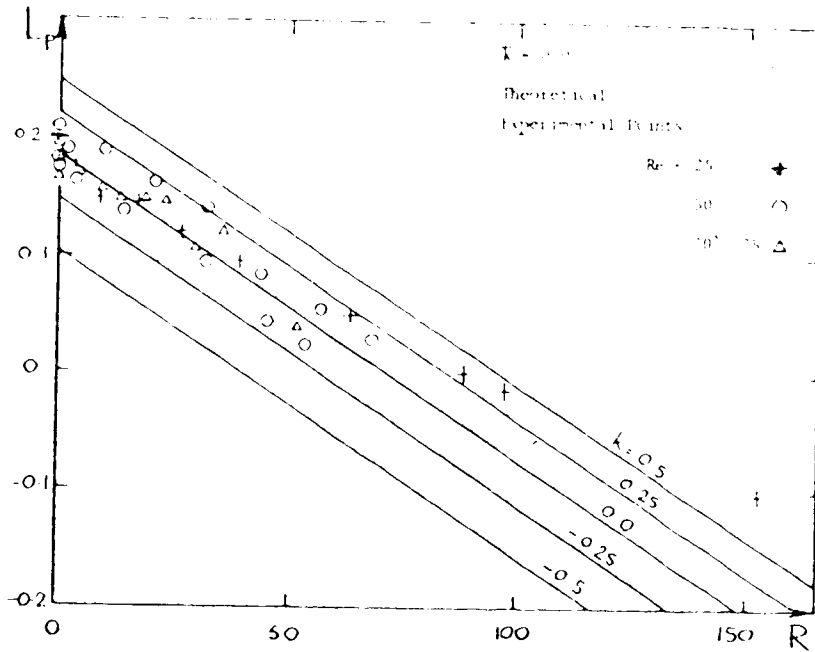


Figure V.9 Dimensionless Load Capacity For Constant Gap Bearing

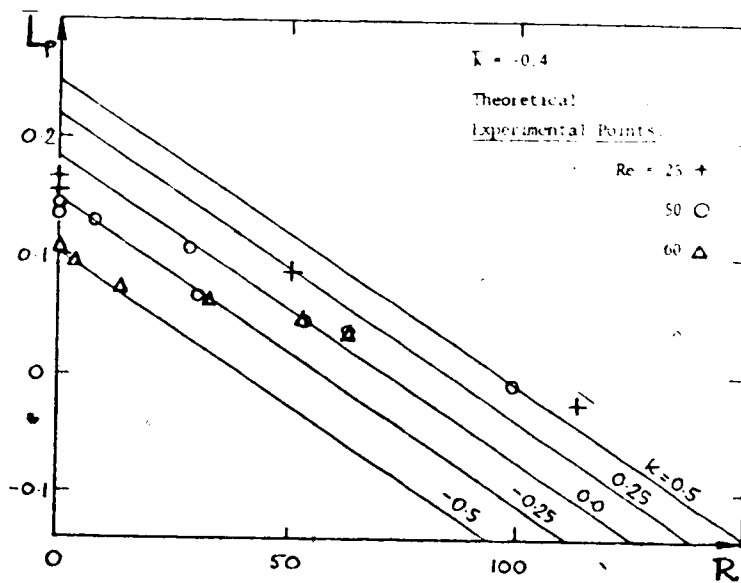


Figure V.10 Dimensionless Load Capacity For Convergent Gap Bearing

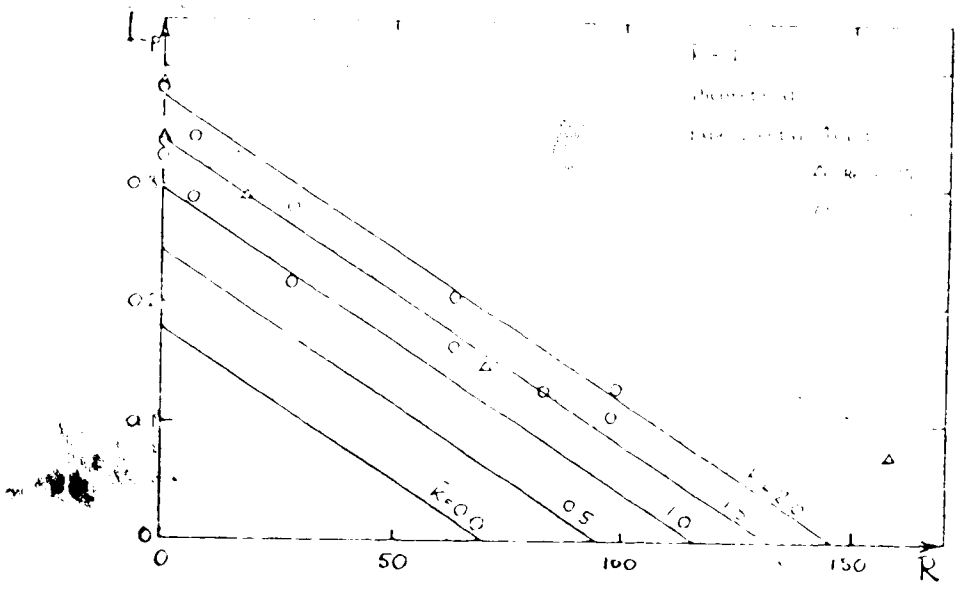


Figure V.11 Dimensionless Load Capacity For Divergent Gap Bearing

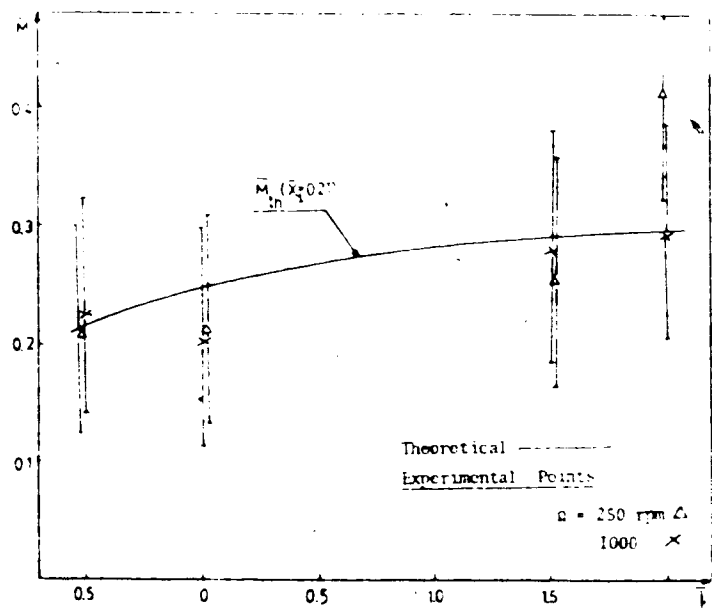


Figure V.12 The Torque Of The Conical Bearing

VI. Observations

In this thesis an experimental investigation of conical bearings with narrow gaps has been described and the results reported. For the bearings considered the lubricant film thickness was very small compared with the length of the bearing gap and as a result the value of λ was much less than 1. For such narrow gaps the pressure distribution along the bearing gap was found to reach very large values which resulted in high load carrying capacities.

For the bearings with non-constant film thicknesses, the difference between the cone angle of the slider and the pad was very small, approximately 1° . One might wonder if small difference of this order would produce any change in the bearing's load capacity and its torque from that of the constant gap bearing.

The recent theoretical analysis {14} of the flow in the bearing, with non-constant lubricant film thickness along the gap, predicted the effects of such a geometry on the load capacity and the torque. It was found that while the gap was relatively wide, approximately 0.1 of the length along the gap, the slight convergence or divergence of the gap did not influence the characteristics of the bearing with respect to constant gap geometry. On the other hand when the gap was very narrow, of order of 0.01 of the length along the gap, the load capacity and the torque of the convergent and divergent gap bearings differed greatly from the values predicted for the constant gap bearings. Quantitatively, for

the convergent gap with $k=-0.5$ the decrease of the load capacity was greater than 40% while the torque decrease was about 15% compared with the values for the constant gap.

The load capacity for the divergent gap (at $\epsilon=0.01$ and $k=2$) increased up to 100% as compared with the constant gap value. In that later case the predicted increase of torque was 20%. However the theory presented in {14} was based on many assumptions simplifying the governing laminar flow equations and experimental data for comparison was required.

During the course of the experiments for small values of the rotational parameter R , the experimental pressure distribution, load capacity and the torque for the constant gap bearing were in a close agreement with the theory (Figs. V.2, 8, 11)

With increasing rotational velocity the pressure values along the gap and consequently the bearing load capacity decreased compared with non-rotational conditions. However with significantly large R parameter and when the pressure along the most part of the gap was less than the outlet pressure, the experimental values of the pressure were higher than the theoretically predicted values and the pressure profiles was found to differ from the theoretical ones (Fig. V.5). The occurrence of flow separation, theoretically predicted in Chapter 3, was thought to be responsible for this effect. Similarly the experimental values of the load capacity were also higher than the theoretical values for increasing values of the rotational

parameter R (Fig. V.9).

The same effects (on the pressure distribution and the load capacity) were found for divergent gap bearing. However the experimental torque values were 10 to 20% higher than theoretically predicted values for $k=1.5$ and 2.

For the convergent gap bearing, the experimental values of the pressure along the gap were higher than the values predicted by theory. As a result the experimental load capacity of this bearing was not much less than the load capacity for constant gap bearing geometry, which was contrary to the theory. The experimental values of the torque, for the convergent bearing geometry, were also higher than theoretically predicted by approximately 20%.

In the range of the geometrical parameter k used during the experiments no evident relationship between the torque and R was found (as predicted by the theoretical analysis).

Although no turbulence was detected during the experiments, one should not forget that the turbulence probe was located at the outlet of the bearing gap, only one of the locations where the turbulence was most likely to occur.

From the practical point of view, according to the results obtained in this thesis it is recommended that the the conical bearing designers should set the manufacturing tolerances to obtain divergent bearing gaps rather than convergent.

Suggestions For Further Work

1. It would be of interest to obtain the flow characteristics of the conical bearing for Reynolds numbers over 100 and to determine the transition from laminar to turbulent flow in the bearing gap.
2. Repeat the same test with bearing slider having free axial displacement.
3. Perform an experimental investigation of the thermal effects on the conical bearing performance.

Table 3. Dimensionless Pressure Distribution for Constant Gap Bearing ($k=0$)

$Re=72$, $h_0=0.65\text{mm}$

$Q(\text{l/sec})$, $T(^{\circ}\text{C})$, $R=Re_{\omega}'/Re$

\bar{P}_1	946.56	934.56	979.95	950.36	1008.51
\bar{P}_2	705.38	687.37	714.69	672.96	698.01
\bar{P}_3	512.37	496.09	518.33	471.46	470.52
\bar{P}_4	358.14	337.36	352.29	311.05	305.44
\bar{P}_5	221.05	203.49	211.97	179.52	172.36
\bar{P}_6	100.03	92.32	96.45	81.40	77.49
R	0.00	0.65	2.80	7.40	17.80
Q	0.038	0.038	0.036	0.036	0.034
T	25.00	25.00	25.50	26.00	27.00

Table 4. Dimensionless Pressure Distribution for Constant Gap Bearing ($k=0$)

$Re=25$, $h_0=0.85\text{mm}$

$Q(\text{l/sec})$, $T(^{\circ}\text{C})$, $R=Re_{\omega}^2/Re$

\bar{P}_1	352.79	321.26	302.06	219.65	140.47
\bar{P}_2	264.59	228.03	202.18	110.84	40.35
\bar{P}_3	206.32	157.20	128.48	50.57	-17.36
\bar{P}_4	134.48	109.21	80.48	16.34	-41.88
\bar{P}_5	90.48	69.00	48.48	5.61	-34.73
\bar{P}_6	50.08	37.92	28.12	11.74	-7.66
R	0.00	9.00	26.50	63.40	97.00
Q	0.015	0.015	0.015	0.014	0.014
T	27.00	27.00	27.50	28.00	28.00

Table 5. Dimensionless Pressure Distribution for Constant Gap Bearing ($k=0$)

$Re=50$, $h_0=0.85\text{mm}$

$Q(\text{l/sec})$, $T(^{\circ}\text{C})$, $R=Re_{\omega}^2/Re$

\bar{P}_1	693.68	663.55	619.62	528.18	285.56
\bar{P}_2	518.99	494.47	434.70	331.00	128.18
\bar{P}_3	365.74	351.95	297.29	202.28	53.22
\bar{P}_4	260.51	239.06	192.06	120.04	2.23
\bar{P}_5	168.56	149.66	117.48	66.91	-10.87
\bar{P}_6	85.81	75.09	60.27	38.31	0.00
R	0.00	3.50	14.00	31.40	53.50
Q	0.029	0.029	0.029	0.027	0.027
T	28.00	28.00	28.00	28.00	29.00

Table 6. Dimensionless Pressure Distribution for Constant Gap Bearing ($k=0$)

$Re=70$, $h_0=0.85\text{mm}$

$Q(\text{l/sec})$, $T(^{\circ}\text{C})$, $R=Re_{\omega}^2/Re$

\bar{P}_1	993.94	981.14	929.05	924.06	852.04
\bar{P}_2	740.31	713.35	658.97	624.72	557.81
\bar{P}_3	547.92	516.39	472.52	420.40	349.90
\bar{P}_4	378.38	354.62	306.18	269.71	210.45
\bar{P}_5	237.63	213.41	190.56	156.31	113.91
\bar{P}_6	120.18	103.27	91.36	77.13	55.16
R	0.00	2.30	9.00	22.70	35.40
Q	0.043	0.043	0.043	0.041	0.041
T	27.00	27.00	27.00	28.00	28.00

Table 7. Dimensionless Pressure Distribution for Constant Gap Bearing ($\bar{k}=0$)

$Re=25$, $h_0=1mm$

$Q(1/sec)$, $T(^{\circ}C)$, $R=Re_w^2/Re$

\bar{P}_1	338.65	335.83	267.95	155.54	-62.57
\bar{P}_2	265.13	231.19	162.61	55.85	-130.69
\bar{P}_3	170.39	128.67	96.86	-04.24	-144.15
\bar{P}_4	150.59	117.36	68.58	-12.72	-92.67
\bar{P}_5	98.27	75.66	41.00	-14.84	-43.56
\bar{P}_6	55.85	40.29	24.03	4.94	1.58
R	0.00	14.10	39.30	88.50	152.50
Q	0.017	0.017	0.017	0.017	0.016
T	28.00	28.00	28.00	28.00	29.00

Table 8. Dimensionless Pressure Distribution for Constant Gap Bearing ($\bar{k}=0$)

$Re=50$, $h_0=1mm$

$Q(1/sec)$, $T(^{\circ}C)$, $R=Re_{\omega}^2/Re$

\bar{P}_1	695.12	654.01	559.76	499.15	377.54
\bar{P}_2	507.90	455.40	368.11	294.82	180.28
\bar{P}_3	368.11	344.08	244.14	162.61	53.02
\bar{P}_4	271.34	234.02	171.40	106.75	24.74
\bar{P}_5	173.30	144.21	102.46	55.85	-28.98
\bar{P}_6	83.49	67.04	50.60	31.81	2.40
R	0.00	4.40	17.60	44.30	68.00
Q	0.036	0.036	0.036	0.036	0.036
T	27.00	27.00	27.00	28.00	28.00

Table 9. Dimensionless Pressure Distribution for Constant Gap Bearing ($k=0$)

$Re=75$, $h_0=1mm$

$Q(l/sec)$, $T(^{\circ}C)$, $R=Re_{\omega}^2/Re$

\bar{P}_1	1159.50	1083.85	996.18	830.74	534.64
\bar{P}_2	850.53	777.00	691.45	540.86	278.01
\bar{P}_3	616.51	545.81	465.21	335.83	119.60
\bar{P}_4	438.34	383.90	321.69	216.34	57.82
\bar{P}_5	279.27	242.50	198.67	125.14	19.00
\bar{P}_6	141.40	120.89	96.86	60.80	8.71
R	0.00	3.28	13.10	29.50	51.60
Q	0.051	0.051	0.051	0.051	0.049
T	28.00	28.00	28.00	28.00	29.00

Table 10. Dimensionless Pressure Distribution for Convergent Gap Bearing ($k=-0.5$)

$Re=25$, $h_o=0.76\text{mm}$

$Q(\text{l/sec})$, $T(^{\circ}\text{C})$, $R=Re_w^t/Re$

\bar{P}_1	238.07	224.89	207.89	164.15	115.16
\bar{P}_2	209.67	194.73	175.25	130.21	82.89
\bar{P}_3	181.55	161.35	142.61	103.45	57.58
\bar{P}_4	149.93	129.14	108.67	76.04	35.93
\bar{P}_5	113.62	94.87	78.00	50.58	23.68
\bar{P}_6	65.80	52.71	41.77	29.04	16.74
R	0.00	4.00	17.90	40.20	78.40
Q	0.015	0.015	0.014	0.014	0.013
T	25.00	25.00	26.00	26.00	28.00

Table 11. Dimensionless Pressure Distribution for Convergent
Gap Bearing ($k=-0.5$)

$Re=50$, $h_0=0.76\text{mm}$

$Q(\text{l/sec})$, $T(^{\circ}\text{C})$, $R=Re_{\omega}/Re$

P_1	448.26	426.71	404.06	338.66	283.13
\bar{P}_2	400.40	372.64	352.54	291.90	235.27
\bar{P}_3	344.87	313.45	299.57	238.92	192.53
\bar{P}_4	389.08	351.08	314.55	252.08	204.42
\bar{P}_5	320.76	285.32	257.92	210.79	164.76
\bar{P}_6	215.18	192.89	181.20	156.36	137.00
R	0.00	2.50	10.00	22.50	35.00
Q	0.027	0.027	0.027	0.027	0.027
T	27.00	27.00	27.00	27.00	27.00

Table 12. Dimensionless Pressure Distribution for Convergent
Gap Bearing ($k=-0.5$)

$Re=75$, $h_0=0.76\text{mm}$

$Q(\text{l/sec})$, $T(^{\circ}\text{C})$, $R=Re_w^2/Re$

P_1	584.00	630.77	588.31	523.59	469.12
P_2	512.04	552.00	507.48	455.06	399.72
P_3	436.70	460.00	420.80	372.19	327.97
P_4	354.57	367.21	334.71	295.17	254.18
P_5	262.80	268.53	241.88	210.55	183.90
P_6	147.56	147.00	132.65	115.08	102.78
R	0.00	1.34	5.34	12.00	18.40
Q	0.049	0.046	0.046	0.046	0.046
T	24.00	25.00	25.00	25.00	25.00

Table 13. Dimensionless Pressure Distribution for Convergent
Gap Bearing ($k=-0.4$)

$Re=25$, $h_0=1.14\text{mm}$

$Q(\text{l/sec})$, $T(^{\circ}\text{C})$, $R=Re_{\omega}^{\prime}/Re$

P_1	303.21	258.37	138.74	-11.94	-83.07
P_2	259.11	219.25	107.50	-31.24	-95.62
P_3	217.76	184.25	85.45	-37.67	-76.31
P_4	177.00	148.22	68.91	-25.72	-29.94
P_5	135.98	116.31	58.80	-11.02	-07.92
P_6	86.37	77.20	48.69	11.02	11.02
R	0.00	14.10	50.03	113.20	185.30
Q	0.019	0.018	0.019	0.019	0.019
T	28.00	29.00	28.00	28.00	28.00

Table 14. Dimensionless Pressure Distribution for Convergent
 Gap Bearing $k = 0.4$
 $Re = 50$, $h_0 = 0.04mm$
 $Q(1/sec)$, $T(°C)$, $P = Re/Re$

P_1	417.92	400.43	339.69	152.34	38.08
P_2	351.00	336.60	272.78	98.81	81.32
P_3	290.28	272.78	219.15	63.82	-88.52
P_4	234.69	220.28	177.05	54.55	-63.82
P_5	173.96	162.64	138.96	53.52	-24.70
P_6	106.02	97.79	90.58	52.49	13.38
R	0.00	7.05	28.20	63.40	98.80
Q	0.037	0.037	0.037	0.037	0.037
T	29.00	29.00	29.00	29.00	29.00

Table 15. Dimensionless Pressure Distribution for Convergent
Gap Bearing ($k = 0.4$)

$Re = 60$, $h_0 = 0.14$ mm

Q (l/sec), T ($^{\circ}C$), $R = Re / Re$

P_1	363.70	319.11	288.61	278.64	215.45
P_2	300.93	254.59	232.29	214.11	144.95
P_3	246.37	214.11	183.61	163.66	99.49
P_4	201.20	162.49	141.96	126.70	83.33
P_5	148.41	115.56	102.65	95.03	65.22
P_6	95.03	72.74	62.18	59.24	48.75
R	0.00	3.35	13.40	30.10	52.70
Q	0.060	0.060	0.060	0.060	0.055
T	24.00	24.00	24.00	24.00	25.00

Table 16. Dimensionless Pressure Distribution in the Divergent Gap Bearings ($k=1.0$)
 $Re=25$, $h_0=0.06mm$
 (a) $se=0.015$, $T=25$, $R=Re_0/Re$

P_1	1572.15	1508.19	1392.17	1372.14	1427.17
P_2	722.72	554.04	383.32	242.81	110.69
P_3	359.31	191.51	38.06	-113.57	-150.88
P_4	185.65	45.38	-76.73	-190.92	322.22
P_5	92.24	-11.75	-85.21	-157.90	-234.91
P_6	38.36	-4.39	-43.92	-63.64	-75.98
R	0.00	4.00	16.00	40.20	70.10
Q	0.015	0.015	0.015	0.014	0.014
T	25.00	25.00	25.00	26.00	26.00

Table 10. Dimensionless Pressure Distribution for Divergent Gap Bearing ($k=2.00$)

$Re=50$, $h=0.76mm$

$z=1$ section, $T=24.00$, $R=Re/Re_0$

P_1	2834.2	2729.9	2650.9	2642	2631.4
P_2	1434.2	1321	1179.7	1087.8	976.02
P_3	840.03	736.80	615.55	480.25	388.59
P_4	383.77	286.78	168.42	36.60	-36.31
P_5	217.69	148.08	74.00	-21.96	-61.78
P_6	130.09	76.39	45.88	15.22	-2.92
R	0.00	1.80	7.13	18.00	28.10
Q	0.033	0.033	0.033	0.031	0.031
T	24.00	24.00	24.00	25.00	25.00

Table 18. Dimensionless Pressure Distribution for Divergent Gap Bearing ($k=2.00$)

$Re=68$, $h_c=0.76mm$

$Q(1 \text{ sec})$, $T(^{\circ}C)$, $R=Re_{\omega} / Re$

P_1	3903.6	3700.9	3622.2	3554.7	3806.8
P_2	2024.4	1792	1655.6	1471.2	1494.5
P_3	1211.4	1006.8	854.73	699.71	658.33
P_4	553.83	378.25	256.61	125.97	21.18
P_5	309.38	198.75	107.69	17.29	-47.85
P_6	168.40	112.26	74.41	29.04	11.32
R	0.00	1.64	6.56	14.80	25.80
Q	0.039	0.039	0.039	0.039	0.038
T	26.00	26.00	26.00	26.00	27.00

Table 19. Dimensionless Pressure Distribution for Divergent Gap Bearing ($k=1.5$)

$Re=25$, $h_0=1.27\text{mm}$

$Q(\text{l sec})$, $T(^{\circ}\text{C})$, $R=Re \int_{Re}^{\infty} Re$

\bar{P}_1	861.13	744.20	648.50	546.11	444.20
\bar{P}_2	570.90	438.33	363.20	273.10	187.66
\bar{P}_3	327.34	255.78	144.46	108.00	89.67
\bar{P}_4	294.56	222.51	30.78	-33.12	-39.74
\bar{P}_5	198.34	135.60	24.44	-39.11	-48.21
\bar{P}_6	165.77	108.55	30.56	21.73	3.59
R	0.00	17.50	69.90	157.20	208.66
Q	0.021	0.021	0.021	0.021	0.021
T	29.00	29.00	29.00	29.00	29.00

Table 20. Dimensionless Pressure Distribution for Divergent Gap Bearing ($k=1.5$)

$Re=50$, $h_o=1.27\text{mm}$

$Q(\text{l/sec})$, $T(^{\circ}\text{C})$, $R=Re_{\omega}^2/Re$

\bar{P}_1	1542.77	1386.54	1284.65	1068.44	1002.11
\bar{P}_2	936.88	804.23	654.22	552.21	426.78
P_3	624.44	582.31	420.99	306.77	174.08
\bar{P}_4	456.56	396.77	294.34	174.33	78.00
\bar{P}_5	336.63	288.87	204.40	144.34	78.67
P_6	270.87	234.56	174.41	142.24	72.68
R	0.00	6.98	27.90	62.85	97.89
Q	0.046	0.046	0.046	0.046	0.046
T	27.00	27.00	27.00	27.00	27.00

Table 2. Dimensionless Torque

$\bar{\Omega}$ (rpm) →	250	500	750	1000
	$\bar{K} = 0.5$		$Re = 50$	
$\frac{R}{M}$	2.5 0.213	10.0 0.276	22.5 0.255	35.0 0.221
	$\bar{K} = 0.4$		$Re = 40$	
$\frac{R}{M}$	1.25 0.19	5.0 0.19	11.25 0.201	17.5 0.194
	$\bar{K} = 0.3$		$Re = 75$	
$\frac{R}{M}$	3.23 0.210	12.9 0.212	29.6 0.246	45.2 0.201
	$\bar{K} = 1.5$		$Re = 60$	
$\frac{R}{M}$	5.24 0.247	23.5 0.372	52.8 0.321	82.3 0.278
	$\bar{K} = 2.0$		$Re = 50$	
$\frac{R}{M}$	1.8 0.441	7.13 0.388	18.0 0.324	28.1 0.287

Bibliography

- {1} A. F. Underwood, "Rotating Load Bearings"
ASME Paper 44-A-29
Aut. Ind. Vol.92, #11, 1945
- {2} D. Fuller, "Theory and Practice of Lubrication for Engineers"
McGraw-Hill Book Company, New-York, 1956
- {3} Loeb and Rippel, "Determination of Flow Film and Load Carrying of Hydrostatic Bearings" Trans. ASLE Vol.1, #2, 1958.
- {4} Ching-Sheng Wu "The Three Dimensional Incompressible Laminar Boundary Layer on a Spinning Cone", Appl. Sci. Res. Sec. A, Vol.8, July, 1958.
- {5} F. Kreith, D. Ellis, J. Giesing "An Experimental Investigation of the Flow Engendered by a Rotating Cone", Appl. Sci. Res. Sec. A, Vol. 11, December, 1961.
- {6} Lyman G. Parrat, "Probability and Experimental Errors in Science", 1967.
- {7} H. Schlichting, "Boundary Layer Theory", McGraw-Hill Book Company, New-York, 1968.
- {8} G. Korn, T. Korn, "Mathematical Handbook", McGraw-Hill Book Company, New-York, 1968.
- {9} W. B. Rowe, I. P. O'Donoghue, "The Practical Uses and Advantages of Externally Pressurized Bearings", Machinery and Production Engineering, Vol.116, #2988, 1970.
- {10} Cz. M. Rodkiewicz, A. Mioduchowski, "The Mean Temperature of a Conical Bearing", WEAR, 31, 227-235, 1975.

{11} Cz. M. Rodkiewicz, W. Jedruch, J. Siepko, "Thermal Effects in Conical Bearings", Mec. Eng. Dept. Report, University of Alberta, Edmonton, Alberta, 1978.

{12} E. Salem, F. Khalil, "Thermal and Inertia Effects in Externally Pressurized Conical Oil Bearing", WEAR, 56, 251-264, 1979.

{13} T. J. Prabhu, N. Ganesan, "Characteristics of Conical Hydrostatic Thrust Bearings Under Rotation", WEAR, 73, 95-122, 1981

{14} W. Kalita, J. S. Kennedy, Cz. M. Rodkiewicz, "Effect of Non-Constant Film Thickness on Conical Bearing Characteristics", Mec. Eng. Dept. Report #37, The University of Alberta, Edmonton, Canada, April 1983.

{15} W. Kalita, N. Yegani, Cz. M. Rodkiewicz, J. S. Kennedy, "Experimental Investigations Of The Laminar Flow Characteristics Of Conical Bearings" Mec. Eng. Dept. Report #39, The University of Alberta, Edmonton, Canada, 1983.

Appendix 1.

Experimental Error Estimation

In the reported experiments the resulting pressure distribution was determined for settled bearing geometry, lubricant flow rate and rotational velocity.

While the rotational velocity, the lubricant properties (that is the viscosity and the density), the lubricant flow rate and the angle α were measured with relatively high accuracy (for an error of less than 2%), the setting of the gap geometry was the major source of error (approximately 10%).

The pressure measured with an error of less than 2% by the pressure transducer was strongly depending on the gap size. The dimensionless pressure, depending also on the same parameters, was calculated with an error of 17%.

The error for the power consumption of the bearing was estimated for less than 5%. However for the resulting torque the estimated error was 11%.

The method of "Propagation of Errors" {6} was used to obtain the error estimations.

Appendix 2.

Calculation of Dimensionless Viscous Drag

The dimensional viscous drag was

$$M = 2\pi r_0 \int_{x_1}^{x_2} \cos^2 \alpha \frac{w}{v} dx$$

writing in dimensionless form we obtain

$$M = \frac{2\pi r_0 h_0}{x_0} \int_{x_1}^{x_2} \cos^2 \alpha \frac{w}{v} dx$$

which is the expression (24) obtain in chapter 1.

In the experiments the drag obtained from the power consumption of the bearing was

$$M = P / \omega$$

substituting this expression in (24) we obtain

$$M = \frac{Ph_0}{2\pi r_0 \omega \int_{x_1}^{x_2} \cos^2 \alpha dx}$$

and using

$$P = P_1 - P_0$$

we obtain the expression for viscous drag as

$$M = \frac{(P_1 - P_0) h_0}{2\pi r_0 \omega \int_{x_1}^{x_2} \cos^2 \alpha dx}$$

where

P_1 is the power consumption of the bearing with lubricant flow through the bearing gap and for a particular rotational velocity.

P_0 is the power consumption value obtained without any lubricant in the bearing gap and for the same rotational

we may use the measure μ .